Volume 43 | Number 6 | 21 March 2014 | Pages 1791–1998

Chem Soc Rev

Chemical Society Reviews
www.rsc.org/chemsocrev

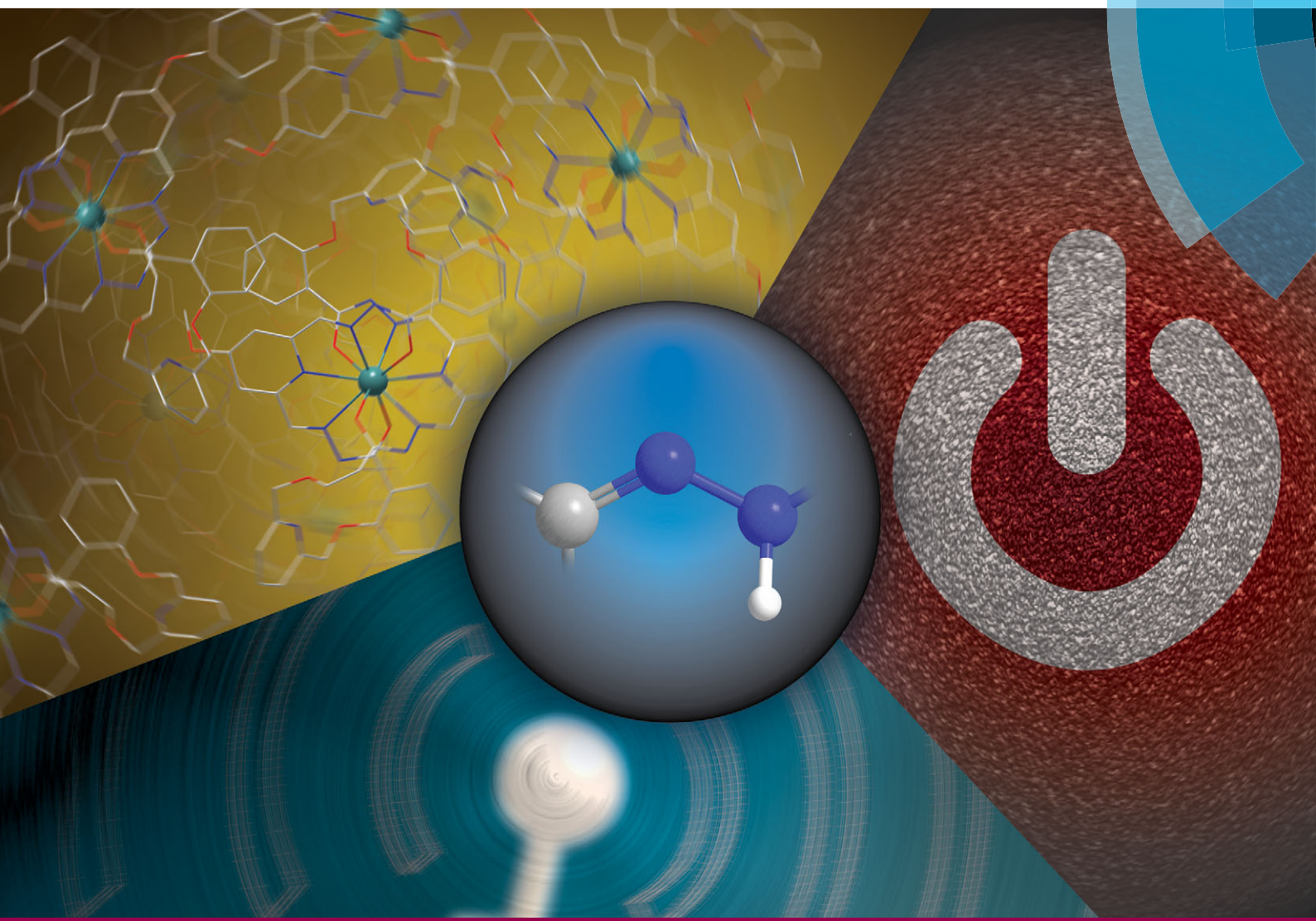

Themed issue: Supramolecular and dynamic covalent reactivity

ISSN 0306-0012

ROYAL SOCIETY OF CHEMISTRY

REVIEW ARTICLE
Xin Su and Ivan Aprahamian
Hydrazone-based switches, metallo-assemblies and sensors

Chem Soc Rev

REVIEW ARTICLE

View Article Online
View Journal | View Issue

Hydrazone-based switches, metallo-assemblies and sensors

Cite this: *Chem. Soc. Rev.*, 2014, **43**, 1963

Xin Su and Ivan Aprahamian*

Received 28th October 2013

DOI: 10.1039/c3cs60385g

www.rsc.org/csr

The hydrazone functional group has been extensively studied and used in the context of supramolecular chemistry. Its pervasiveness and versatility can be attributed to its ease of synthesis, modularity, and most importantly unique structural properties, which enable its integration in different applications. This review provides an overview of the utilization of hydrazones in three supramolecular chemistry related areas: molecular switches, metallo-assemblies and sensors. These topics were chosen because they highlight the diversity of hydrazones, and emphasize their uniqueness *vis-à-vis* the imine functional group. Discussion entails (i) chemical and light activated switching of hydrazones, and how this can be used in controlling the properties of self-assembled systems, (ii) the use of hydrazones in the formation of dynamic and stimuli responsive metallogrids, and (iii) the use of hydrazones in detecting metal cations (Zn^{2+}, Cu^{2+}, Hg^{2+}, *etc.*), anions (F^-, CN^-, $P_2O_7^{4-}$, *etc.*) and neutral molecules (amines, water, Cys, *etc.*).

1 Introduction

The hydrazone functional group is ubiquitous in various fields ranging from organic synthesis[1] and medicinal chemistry[2] to supramolecular chemistry,[3] and has been used in metal and covalent organic frameworks,[4] dynamic combinatorial chemistry (DCC),[5] dye[6] and hole-transporting materials,[7] among other applications.[8] The modularity, straightforward synthesis, and stability towards hydrolysis (*cf.* imines) of hydrazones can be cited as reasons for their popularity. But in reality it is the functional diversity of this azomethine group, which is characterized by the triatomic structure C=N–N, that enables its use in various fields. A quick survey of the structure of a hydrazone (Fig. 1) reveals that it has (i) nucleophilic imine and amino-type (more reactive) nitrogens, (ii) an imine carbon that has both electrophilic and nucleophilic character, (iii) configurational isomerism stemming from the intrinsic nature of the C=N double bond, and (iv) in most cases an acidic N–H proton. These structural motifs give the hydrazone group its physical and chemical properties, in addition to playing a crucial part in determining the range of applications it can be involved in.

Hydrazones can be made by three main synthetic pathways (Scheme 1), (i) coupling between aryl diazonium salts and

Department of Chemistry, Dartmouth College, Hanover, New Hampshire 03755, USA. E-mail: ivan.aprahamian@dartmouth.edu

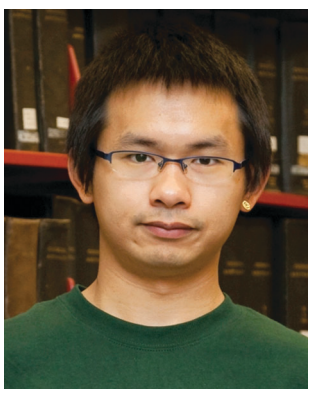

Xin Su

Xin Su received his BS degree in chemistry from Nankai University (2009), where he worked in the Liu group on the recognition and assembly of water-soluble calixarenes. He joined the Aprahamian group at Dartmouth College in 2009, and has since then been working on the development of novel hydrazone-based molecular switches and switching systems thereof. He received his PhD degree in December, 2013.

Ivan Aprahamian

Ivan Aprahamian received all his degrees (BSc – 1998, MSc – 2000, and PhD – 2005) from the Hebrew University of Jerusalem, Israel. His doctoral research was conducted under the supervision of Professors Mordecai Rabinovitz and Tuvia Sheradsky. He started his independent career at Dartmouth College in 2008, after finishing his postdoctoral research with Sir Fraser Stoddart (UCLA). His research focuses on using structurally simple, modular, and tunable hydrazone-based building blocks in the development of adaptive functional materials.

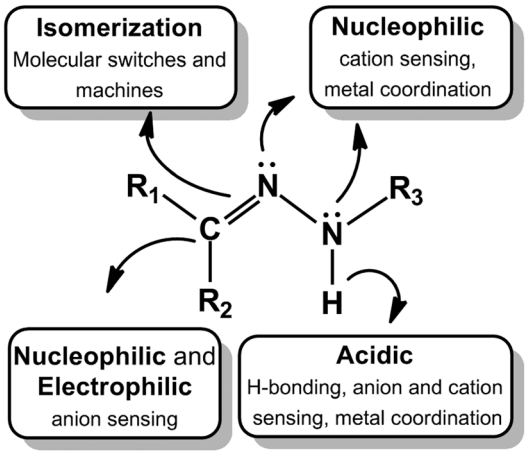

Fig. 1 The structural and functional diversity of the hydrazone group.

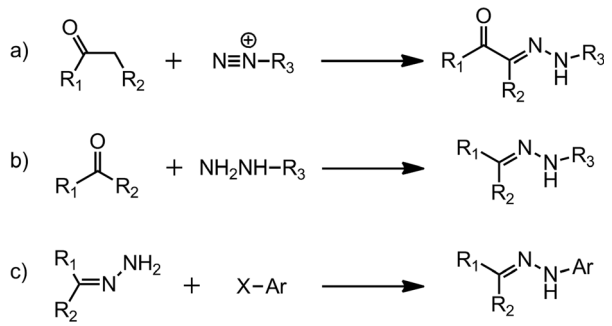

Scheme 1 The synthesis of hydrazones *via* (a) the Japp–Klingemann reaction; (b) hydrazine–ketone/aldehyde condensation; and (c) aryl halide substitution.

β-keto esters or acids, which is also known as the Japp–Klingemann reaction,[9] (ii) coupling between hydrazines and ketones or aldehydes,[10,11] and (iii) coupling between aryl halides and non-substituted hydrazones.[12,13] The readily obtained compounds are usually highly crystalline and crash out of the reaction mixture, which simplifies their purification process and adds to the appeal of these systems.

In this review we will focus on the use of the hydrazone group in: (i) molecular switches,[14] (ii) metallo-assemblies,[15] and (iii) sensing applications,[16] in order to showcase the diversity of this functional group in the context of supramolecular chemistry. In the first section we will focus on the use of light and chemical inputs in activating the *E*/*Z* isomerization in these systems. We will also discuss how the acidic N–H proton in hydrazones differentiates it from imines, by leading for example to a new isomerization mechanism that is not present in the latter. Moreover, we will demonstrate how these structurally simple systems can be used for complex functions, such as controlling the properties of liquid crystals and the morphology of macroscopic assemblies. In the second part we will show how different metallo-assemblies can be formed using different combinations of hydrazone derivatives and metals. Moreover, we will demonstrate how such systems can be stimulated to undergo dynamic shape changes, and be used as metallo-dynamers and gels. Finally, we will show how the nucleophilicity of the hydrazone nitrogens, electrophilicity of the imine carbon, and acidity of the N–H proton can be utilized in highly sensitive and selective sensing of cations, anions and even neutral species. A common theme in all these research directions is the acidic N–H proton, which as discussed below, enables the switching, metal coordination, and sensing applications. This functional group also distinguishes and differentiates the hydrazone from the imine group.

2 Configurational switching

The control of molecular level motion is the primary objective of the field of molecular switches and machines.[14] With time, there will be a need for the incorporation of more and more complicated functions into such systems. This requirement will necessitate the expansion of the currently available tool box in the field, as far as it relates to the type of intricate motions that we can control externally. The hydrazone functional group is perfectly suited to address this challenge as its *E*/*Z* isomerization (*i.e.*, configurational switching) can be activated by both light and chemical inputs. This dual control over the rotary motion of a molecular system showcases the uniqueness of the hydrazone functional group. Here we will summarize some of the recent advances in the use of hydrazones in modulating the motion of molecules and supramolecular systems.

2.1 Photoswitching

The intrinsic nature of the C=N bond leads to configurational isomerism in hydrazones, which can exist in either the *E* or *Z* forms in solution.[17] It has long been established that UV light can provide enough energy for the $E \rightarrow Z$ isomerization of the C=N bond,[18,19] although in most cases the obtained *Z* isomers are ephemeral species. Courtot *et al.*[20] studied the photoisomerization of a series of 1,2,3-tricarbonyl-2-arylhydrazones (TCAHs) derived from β-diketones and β-ketoesters, and found that the less favored *Z* configuration can be stabilized through intramolecular H-bonding, making it kinetically stable (Scheme 2a). These studies have opened the way for the use of hydrazones as photochemically controlled configurational switches. It was proposed by Courtot *et al.*[20] that these systems isomerize through a photo- or thermally-activated rotational mechanism. This finding prompted Tamaki *et al.*[21] to try and use these systems as command molecules for the alignment of liquid crystals (LCs) on surfaces (Scheme 2b). These efforts showed that the configurational switching in hydrazones can indeed be used in switching the LC alignment between homeotropic and parallel modes using light and heat as inputs.

On the other hand, Smirnov *et al.*[22] observed that acyl hydrazones can also undergo photoisomerization, which proceeds through the weakening of the C=N bond by the electronic transition from the π-orbital of the amine moiety to the π*-orbital of the whole molecule, namely, the π_2–π_1* transition. This photoisomerization was observed in the solid state as well.[23]

Lehn *et al.*[24] demonstrated that some pyridyl-2-aldehyde phenylhydrazones (**1–3**) and acyl hydrazones (**7–10**, Scheme 3)

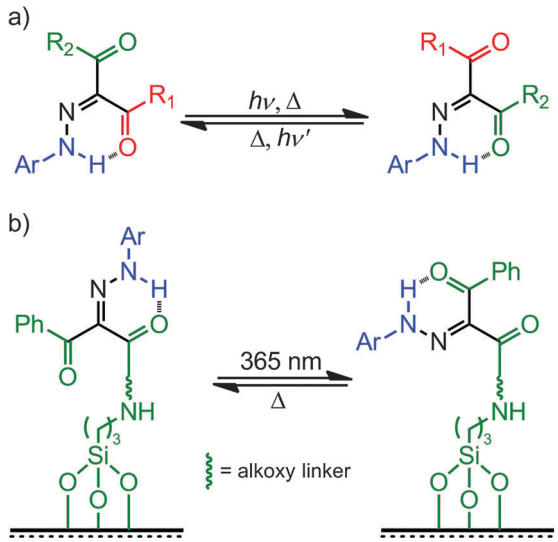

Scheme 2 The photo- and thermal isomerization of TCAHs (a) in solution and (b) on a surface.

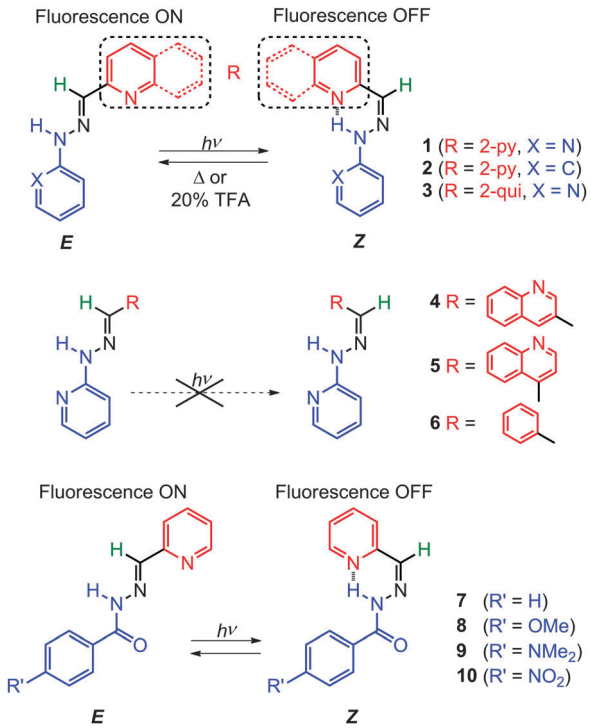

Scheme 3 Photo-induced $E \rightarrow Z$ configurational switching in hydrazones **1–3** and **7–10**.

can also undergo $E \rightarrow Z$ photoisomerization upon UV light irradiation with up to 94% quantum yield (**1-*Z***) in deuterated methanol (CD_3OD). The Z isomers are highly resistant to isomerization because of the intramolecular H-bond; for example, no **1-*E*** can be detected in the CD_3OD solution of **1-*Z*** kept at 45 °C for five days, and only refluxing in CD_3OD or the addition of 20 mol% TFA can regenerate **1-*E*** from **1-*Z***.

On the other hand aryl hydrazones **4–6** (Scheme 3), which are structurally similar to **1–3**, but cannot form intramolecular

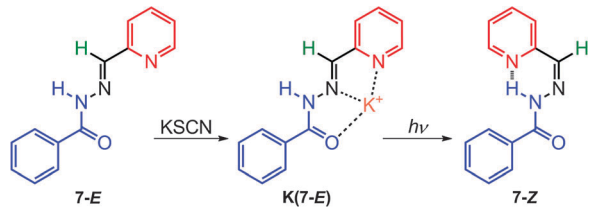

Scheme 4 Photo-induced $E \rightarrow Z$ configurational switching in **K(7-*E*)** with simultaneous release of the K^+ cation.

H-bonds nor can take advantage of their stabilization, do not undergo appreciable $E \leftrightharpoons Z$ photoisomerization. Interestingly, the E isomers of switches **1–3** and **7–10**, are fluorescent, whereas the Z isomers are not. This difference in photophysical properties allows for the toggling of the readout signal using the $E \rightarrow Z$ isomerization process.

As tridentate ligands, the E isomers of hydrazones **1** and **7–10** can coordinate to transition metal cations *via* the NNN and NNO binding sites, respectively. This process locks the E configuration in place. Hence, the binding of **1-*E*** with Zn^{2+} yields the metal complex **Zn(1-*E*)** that cannot undergo photoisomerization. The addition of a free ligand such as tris(2-aminoethyl)amine (Tren) to the mixture regenerates **1-*E*** by removing Zn^{2+}, and unlocks the switch and allows it to photoisomerize again.

In contrast to the stable coordination complex formed between Zn^{2+} and **7–10**, potassium thiocyanate (KSCN) forms a weak 1 : 1 complex with **7** (**K(7-*E*)**), with a binding constant of 24.8 M^{-1} in acetonitrile (Scheme 4).[25] When subjected to UV irradiation, **K(7-*E*)** can be converted into **7-*Z***, accompanied by the simultaneous release of K^+. Upon heating at 40 °C, the isomerization from **7-*Z*** to **7-*E*** is accelerated by a factor of 6 in the presence of 1 equiv. of KSCN, most likely driven by the formation of **K(7-*E*)**. More importantly, complex **K(7-*E*)** forms a crystalline metallo-supramolecular assembly in the presence of SCN^-, which deforms to amorphous stains upon photoisomerization. This process is reversible as the crystals can be regenerated through recrystallization. This study demonstrates how molecular switches can be used in controlling the morphology of macroscopic assemblies.

2.2 pH-activated switching

As mentioned above, TCAHs[20] exist in solution as an equilibrated mixture of intramolecularly H-bonded E and Z isomers (Scheme 5a). The $E \rightarrow Z$ (or *vice versa*) isomerization proceeds *via* hydrazone-azo tautomerization followed by rotation about a C–N single bond. The position of the equilibrium can be altered by catalytic amounts of acid and base, albeit the process does not proceed to full completion, because the H-bond accepting capability of the two carbonyl groups is similar, providing insufficient impetus to drive the equilibrium to full extent in either direction. This property is of course not ideal for molecular switch related applications.

The replacement of one of the carbonyl groups in TCAHs with a pyridyl group, a much stronger H-bond acceptor (*e.g.*, **11** and **12**), has led to systems having an appreciable bias in favor

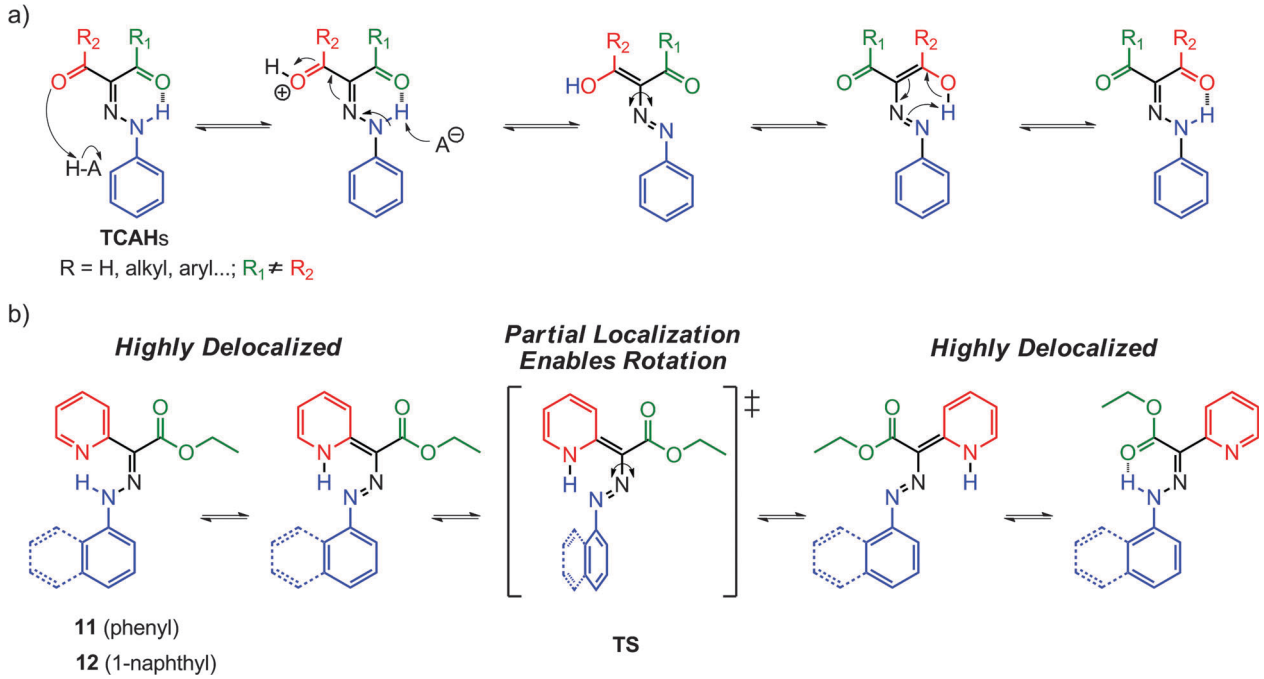

Scheme 5 (a) Possible mechanism for the acid-catalyzed tautomerization in TCAHs (a similar mechanism applies to the base catalyzed process); (b) the proposed tautomerization followed by rotation mechanism in switches **11** and **12**, with intermediates and the transition state (TS) structure.

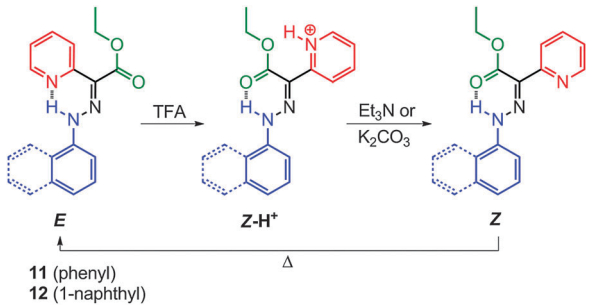

Scheme 6 The acid–base modulated $E \rightleftharpoons Z$ switching in **11** and **12**.

of the *E* configuration (Scheme 6).[26,27] The basic nature of the pyridyl group allows for the modulation of its H-bond accepting ability using acid input, which in turn makes the *Z* isomer the sole configuration upon protonation. This approach has provided prototypical molecular switches that can be fully, effectively, and reversibly switched between the *E* and *Z* configurations, using acid and base inputs.

Compounds **11** and **12** have high *E*:*Z* isomer ratios (93:7 and 97:3, respectively), in deuterated acetonitrile (CD_3CN), indicating that the *E* isomers are more stable than the *Z* ones by 1.5 and 2.0 kcal mol^{-1}, respectively (Scheme 6). Similar to TCAHs, the energy barrier for the interconversion between the *E* and *Z* isomers of **11** and **12** falls within the timeframe of ^{1}H NMR spectroscopy (*ca.* 24 kcal mol^{-1}), leading to two sets of signals in the ^{1}H NMR spectrum. The signals are usually very well separated, especially those for the intramolecular H-bonded N–H protons, which usually have a *ca.* 2 ppm upfield shift going from the *E* to *Z* isomer. Compounds **11-*E*** and **12-*E*** can be converted quantitatively to **11-*Z*-H$^+$** and **12-*Z*-H$^+$**, respectively, upon treatment with trifluoroacetic acid (TFA). When **11-*Z*-H$^+$** and **12-*Z*-H$^+$** are passed over a plug of K_2CO_3, the "metastable" *Z* isomers (**11-*Z*** and **12-*Z***) are observed, which thermally equilibrate to give back **11-*E*** and **12-*E*** in their original isomer ratios, thus completing a full switching cycle.

Mechanistic studies have shown that **11-*E*** and **12-*E*** form the kinetic intermediates **11-*E*-H$^+$** and **12-*E*-H$^+$**, respectively, upon protonation before isomerizing into **11-*Z*-H$^+$** and **12-*Z*-H$^+$** *via* a single rate limiting step. The first-order rate constants of the $Z \rightarrow E$ process (Scheme 6) show dependence on solvent polarity with the associated enthalpies of activation ranging from −30 to −60 kcal mol^{-1}. Based on calculations, these results stem from an increase in the dipole moments of the transition states as compared to the ground states. These data, in conjugation with the DFT calculations, led to the proposal of a tautomerization followed by rotation mechanism for the $E \leftrightharpoons Z$ isomerization in these systems (Scheme 5b).

The delicate balance between the two anchors (*i.e.*, the pyridyl and ester H-bond acceptors) in the rotor part proves to be crucial for the efficient function of the switches.[28] Replacing the ester group in **11** with hydrogen (**13**), a methyl (**14**) or a cyano (**15**) group leads to a dominant configuration in which the pyridyl ring is not involved in H-bonding (Scheme 7). On the other hand, the substitution with an acetyl group (**16**) leads to incomplete acid-activated switching. These results show that a moderate H-bond acceptor is necessary to ensure the correct isomer ratio and switching efficiency in these systems.

Replacing the 1-naphthyl ring in **12** with an 8-quinolinyl one leads to the tristable switch **17** (Scheme 8).[29] The introduction of an additional H-bond acceptor (quinolinyl nitrogen) in the

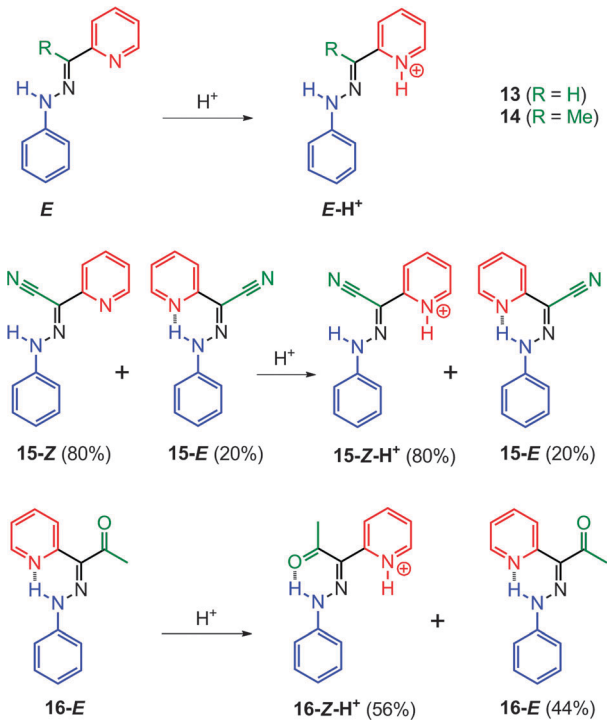

Scheme 7 2-Pyridylarylhydrazones **13–16** with different rotors (only the stable isomer(s) in solution and their protonation products are shown).

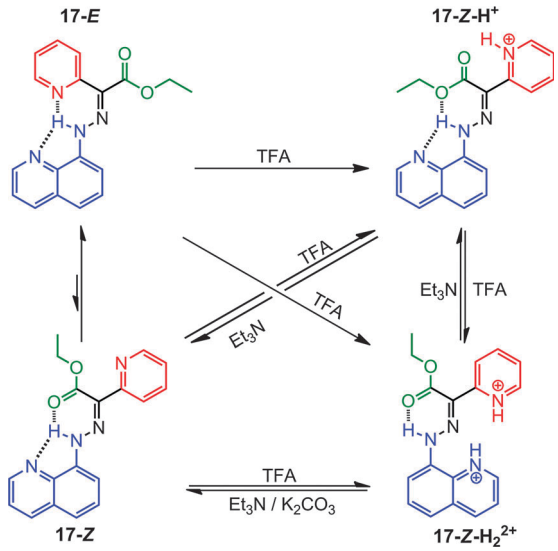

Scheme 8 The acid–base induced configurational and conformational switching in **17**.

stator moiety locks its conformation and opens the way to control its position as a function of pH (*i.e.*, rotation around the C–N bond upon protonation).

The initial protonation of **17-*E*** by TFA leads to **17-*Z*-H$^+$** through a configurational change (*i.e.*, rotation around the C=N bond) because pyridyl is a stronger base than quinolinyl (Scheme 8). Further protonation leads to rotation about the C–N single bond generating a new conformational isomer, **17-*Z*-H$_2^{2+}$**, that *retains* the *Z* configuration. After deprotonation with K_2CO_3 or triethylamine (Et_3N), both **17-*Z*-H$^+$** and **17-*Z*-H$_2^{2+}$** convert into a neutral metastable species **17-*Z***, which eventually equilibrates to give back the thermodynamically stable **17-*E*** isomer.

The configuration and conformation of the system can be modulated based on the sequence in which the acid and base are added, leading to a switch that can be prompted to perform precisely controlled rotations around two different axles. Therefore, a molecular choreography can be achieved by programming the quantity of acid and base used, leading to complicated sequences of rotations in **17**.

2.3 Switching *via* coordination-coupled deprotonation (CCD)

Coordination-coupled deprotonation (CCD) is a process commonly observed in biological systems whereupon the coordination of transition metals with protein residues leads to the release of proton(s) to the environment.[30] CCD provides a great potential for operating chemically activated molecular switches under mild or neutral conditions.[31,32]

Switch **17-*E*** can bind to Zn^{2+} through its quinolinyl and hydrazone N–H nitrogens, leading to the deprotonation of the latter, and subsequent transfer of the proton to the pyridyl nitrogen (Scheme 9).[31] Overcrowded in a positively charged environment, the protonated pyridyl group is forced to rotate around the C=N bond, leading to the coordination of Zn^{2+} with the ester group (**Zn(17-*Z*)**). Tetra-*n*-butylammonium cyanide (*n*Bu_4NCN) can then be used in removing Zn^{2+} from **Zn(17-*Z*)**, which regenerates **17-*E***, and renders the switching process fully reversible.

As an orthogonal input for switches that are only responsive to protons (*e.g.*, **11**), Zn^{2+} can be used to turn CCD-activated switches into proton sources for subsequent switching events.[32] This has been demonstrated with **18**, which is similar to switch **17** but has a methylimidazolyl group in the rotor instead of a pyridyl one (Scheme 10). As in the case of **17**, the binding with Zn^{2+} converts **18-*E*** into **Zn(18-*Z*-H$^+$)**, and when this switching process occurs in the presence of **11-*E***, it yields **Zn(18-*Z*)** and **11-*Z*-H$^+$**. Interestingly, **11-*E*** is protonated and switched by a proton relay from **Zn(18-*Z*-H$^+$)**, upgrading a single CCD-activated switching event into a switching cascade. Both **Zn(18-*Z*)** and **11-*Z*-H$^+$** can be reinstated to **18-*E*** and **11-*E***, respectively, using *n*Bu_4NCN (Scheme 10).

Although the only difference between **17** and **18** is the N-heteroaromatic group in the rotor, the switching cascade is

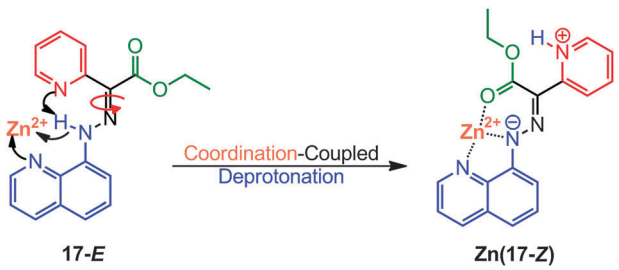

Scheme 9 Proposed mechanism for the *E* → *Z* isomerization of **17** through CCD.

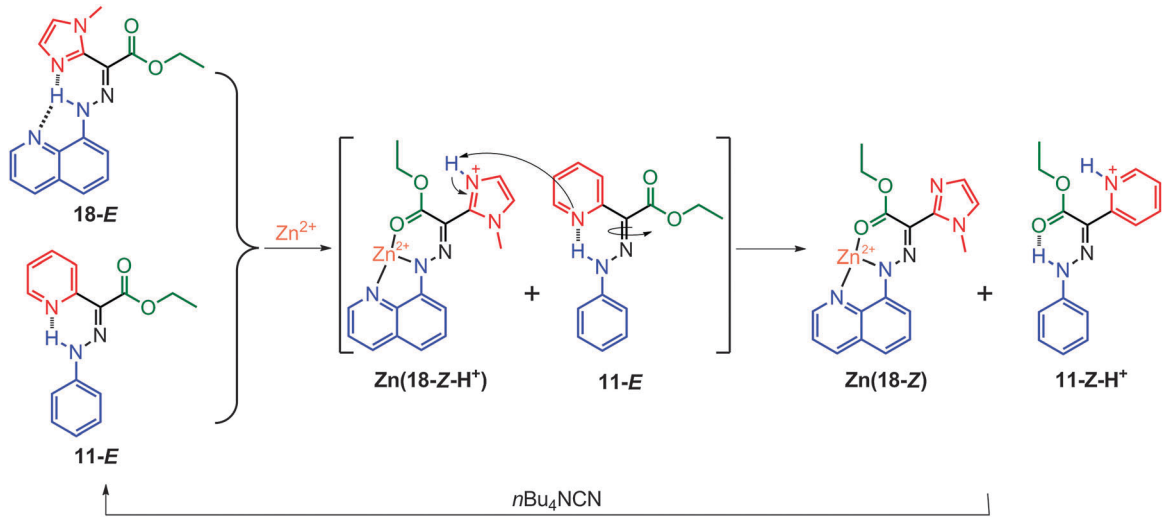

Scheme 10 The reversible switching cascade triggered by Zn^{2+} coordination.

not observed for **17**. In order for the cascade to proceed, there has to be a significant decrease in the basicity of the methyl-imidazolium group in **18** so that it can protonate **11**. The electrostatic repulsion between Zn^{2+} and the imidazolium group results in the required reduction in the pK_a of **Zn(18-*Z*-H$^+$)**. However, this same process happens in **17** as well, and so another factor must be at play. It turns out that the highly planar skeleton in **Zn(17-*Z*)** leads to a very strong H-bonded pyridyl proton, which is not available for proton relay. On the other hand the methyl group in **18** pushes the system out of planarity, leading to a weak H-bonded proton that participates in the switching cascade.

2.4 Switching beyond the molecular level

One of the major objectives of the field of molecular switches and machines is the propagation of the structural changes on the molecular level to dimensional scales beyond their own sizes, *i.e.*, from microscopic to mesoscopic and macroscopic scales.[14]

Liquid crystals are supramolecular assemblies whose properties have been successfully manipulated by photochemically activated switches,[33] and less so by chemically activated ones. Being highly modular, the hydrazone switch **11** can be easily converted into a mesogenic liquid crystalline system (**19**), having a cholesteryl group in each of the rotor and stator parts (Scheme 11).

Hydrazone **19** exists in an *E*/*Z* isomer ratio of 91 : 9 in deuterated dichloromethane (CD_2Cl_2) solution, and exhibits a similar switching behavior to **11** upon exposure to acid/base.[34] DFT calculations using the hybrid B3LYP-D3 (6-31G*) yielded minimum energy structures for **19-*E***, where the cholesteryl units are oriented in a *syn*-fashion (Fig. 2a), and **19-*Z*-H$^+$**, in which the cholesteryl units are oriented in an *anti*-fashion (Fig. 2b). Based on the calculations, the protonation-driven switching process leads to a 10.4% increase in the solvent accessible surface area.

Doping of **19** (5 wt%) into the achiral LC material Nematic Phase 5 (NP5) yields a chiral nematic phase. Upon exposure to TFA, **19**/NP5 (5 wt%) in 90° twisted cells changes its reflected color from green to purple under cross-polarized view (Fig. 2c), accompanied by a decrease in the helical twisting power (HTP) from 56 to 46 μm^{-1} (wt%). The color change can be reversed by exposing the mixture to Et_3N, which also reverts the HTP to 56 μm^{-1} (wt%).

The observed change in the reflected color originates from the structural change in the LC supramolecular assembly brought about by the pH activated rotary motion in the chiral

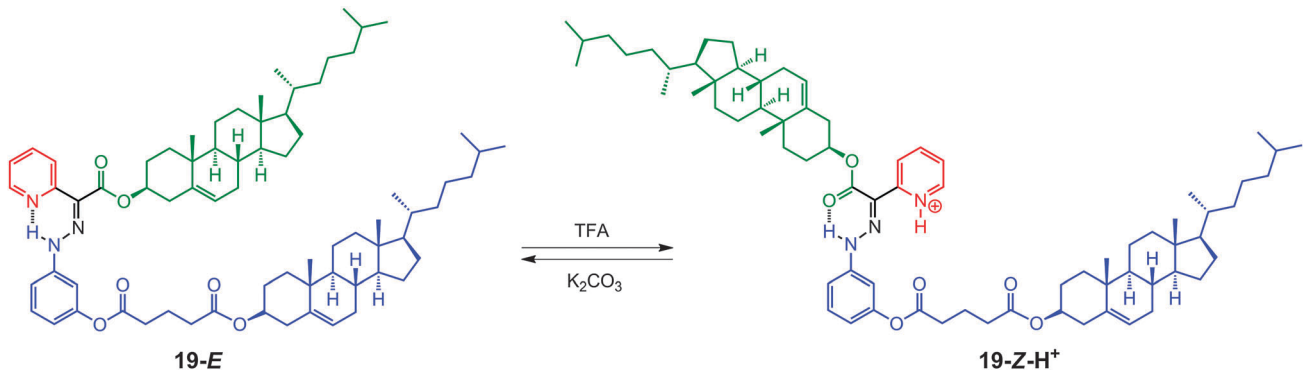

Scheme 11 The acid–base modulated *E* ⇌ *Z* switching in **19**, accompanied by a change in the relative orientation of the cholesteryl units.

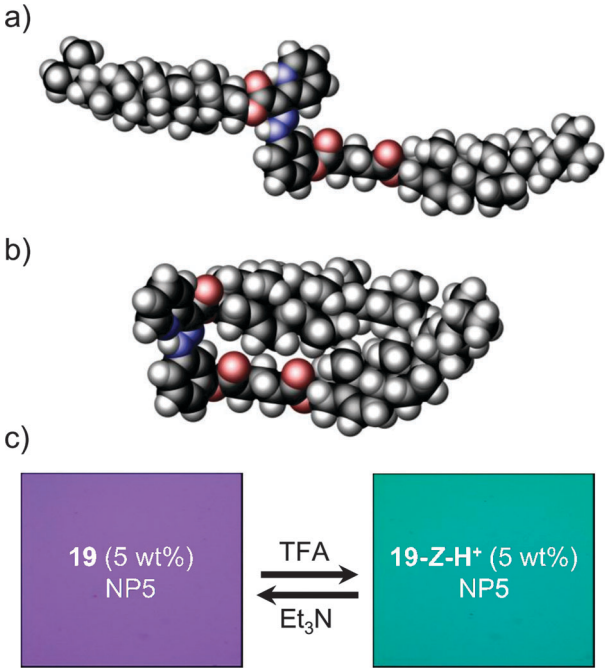

Fig. 2 DFT (B3LYP-D3/6-31G*) calculated structures of (a) **19-*E*** and (b) **19-*Z*-H$^+$**; and, (c) cross-polarized view of the reflected color upon switching **19**/NP5.

switch, and the accompanied increase in the solvent accessible surface area. This process exemplifies the use of a chemically activated molecular switch in effecting mesoscopic level response in bulk materials.

3 Dynamics of hydrazone-based metallo-assemblies

Metallogrids,[15] short for metallosupramolecular grid complexes, are oligonuclear metal complexes where the ligands are connected in the form of square or rectangular grids by spatially well-defined metal cation arrays. Among the variety of molecular scaffolds for building metallogrids, hydrazone-based ligands have been by far the most widely used systems, especially bis-hydrazones connected by symmetric heteroaromatic cores, including pyridine, pyrimidine and triazine. Two recent review articles[3a,15b] have comprehensively covered progresses in the design, synthesis, properties and applications of metallogrids, most of which are hydrazone-based systems (Scheme 12). Hence, we will direct our focus here on the dynamic processes of such metallogrids, such as shape manipulation, stimuli-induced structural interconversion and other dynamic phenomena.

3.1 Dynamic shape adaptation

Oligomeric hydrazone ligands usually exist as contracted helical strands in solution.[35,36] In the presence of large excess of metal cations, these helical coils extend to give linear shaped strands, in order to accommodate the metals. This process can bring about significant changes in the shape of the ligands. Stoichiometry can be a determining factor in controlling the shape of the obtained metalloassemblies, especially when the ligands provide multiple binding modes. For example, ligand **20** forms a [2 × 2] metallogrid[35] $[Pb_4\mathbf{20}_4]^{8+}$ and a double helicate[36] $[Ag_2\mathbf{20}_2]^{2+}$ with 1 equiv. of lead(II) triflate ($Pb(OTf)_2$) and silver(I) tetrafluoroborate ($AgBF_4$), respectively (Fig. 3). When the amount of metal cations is increased, both assemblies lead to the formation of 1 : 2 rack-type linear complexes $[Pb_2\mathbf{20}]^{4+}$ and $[Ag_2\mathbf{20}]^{2+}$. Similarly, the [2 × 2] metallogrid $[Ag_4\mathbf{21}_4]^{4+}$ can be converted into the 1 : 2 linear rack $[Ag_2\mathbf{21}]^{2+}$. Meanwhile, the addition of hydroxymethyl[37,38] and acryloyl[39] groups to the terminal pyridines in bis-hydrazone scaffolds such as in **20**, can also affect the self-assembly behavior. For example, these groups inhibit the formation of [2 × 2] grids by blocking access to the metal centers. Moreover, the hydroxymethyl groups contribute to the extended supramolecular structure of the complexes through metal coordination and H-bonding.[40]

By extending the coordination units in the ligands, the motional shape adaption can be used to form larger assemblies.[35] When ligand **22** is treated with large excess of $Pb(OTf)_2$, the initial [4 × 4] metallogrid $[Pb_{16}\mathbf{22}_8]^{32+}$ turns into a linear complex $[Pb_4\mathbf{22}]^{8+}$ (Fig. 4).

Ligands **23** and **24**[41] on the other hand undergo a three-stage conversion from double pincer to pincer and finally to a linear rack when the corresponding ligand/Pb^{2+} ratios are changed from 1 : 2 to 1 : 1, and then to 2 : 1 (Fig. 5).

Shape modulation can also be achieved by the isosteric modification of binding site geometry in the ligands. For example, ligand **25**[42] is an isosteric isomer of **21**, and although both lead to linear racks upon coordination with Zn^{2+}, **25** has to undergo a "twirling"-type motion, whereas **21** undergoes a "flapping"-type motion. Such effects become more prominent when the ligands grow longer, and have more coordination units, such as in the case of **26** with Pb^{2+} (Fig. 6).

Integrating the bis-hydrazone moiety into macrocycles converts the local shape changes upon coordination into overall conformational switching of the macrocyles.[43] The "S"-shaped 44-membered [2 + 2] macrocycles **27** and **28** each consist of two bis-acylhydrazone units connected by flexible linkers. Upon coordination with La^{3+}, Eu^{3+} and Dy^{3+}, **27** and **28** twist from their "S" conformation to accommodate the metal cations with their two NNNOO-binding units (Fig. 7).

When the element of two-fold symmetry is lost in basic hydrazone ligands, they can potentially be used for preparing homochiral metalloassemblies.[44,45] Hydrazone **4**,[44] studied as a candidate for configurational switching, is also a tridentate ligand that can form a tris-chelated complex $[Fe\mathbf{4}_3]^{2+}$ with iron(II) perchlorate ($Fe(ClO_4)_2$). As a result of the steric hindrance originating from the *C*-methyl group in **4**, $[Fe\mathbf{4}_3]^{2+}$ is obtained only as an optically pure *fac*-*Λ* isomer (Fig. 8). The unsymmetrical bis-hydrazone **29** reacts with mercury(II) triflate ($Hg(CF_3SO_3)_2$) to give both parallel and antiparallel binuclear double helicates $[Hg_2\mathbf{29}_2]^{4+}$ in solution.[45] In the solid state, however, $[Hg_2\mathbf{29}_2]^{4+}$ selectively crystallizes into the antiparallel enantiomeric pair because of the favorable H-bonds and π–π interactions in this structure (Fig. 8).

The addition of other binding features to the hydrazone ligands allows for the construction of high order metalloassemblies.

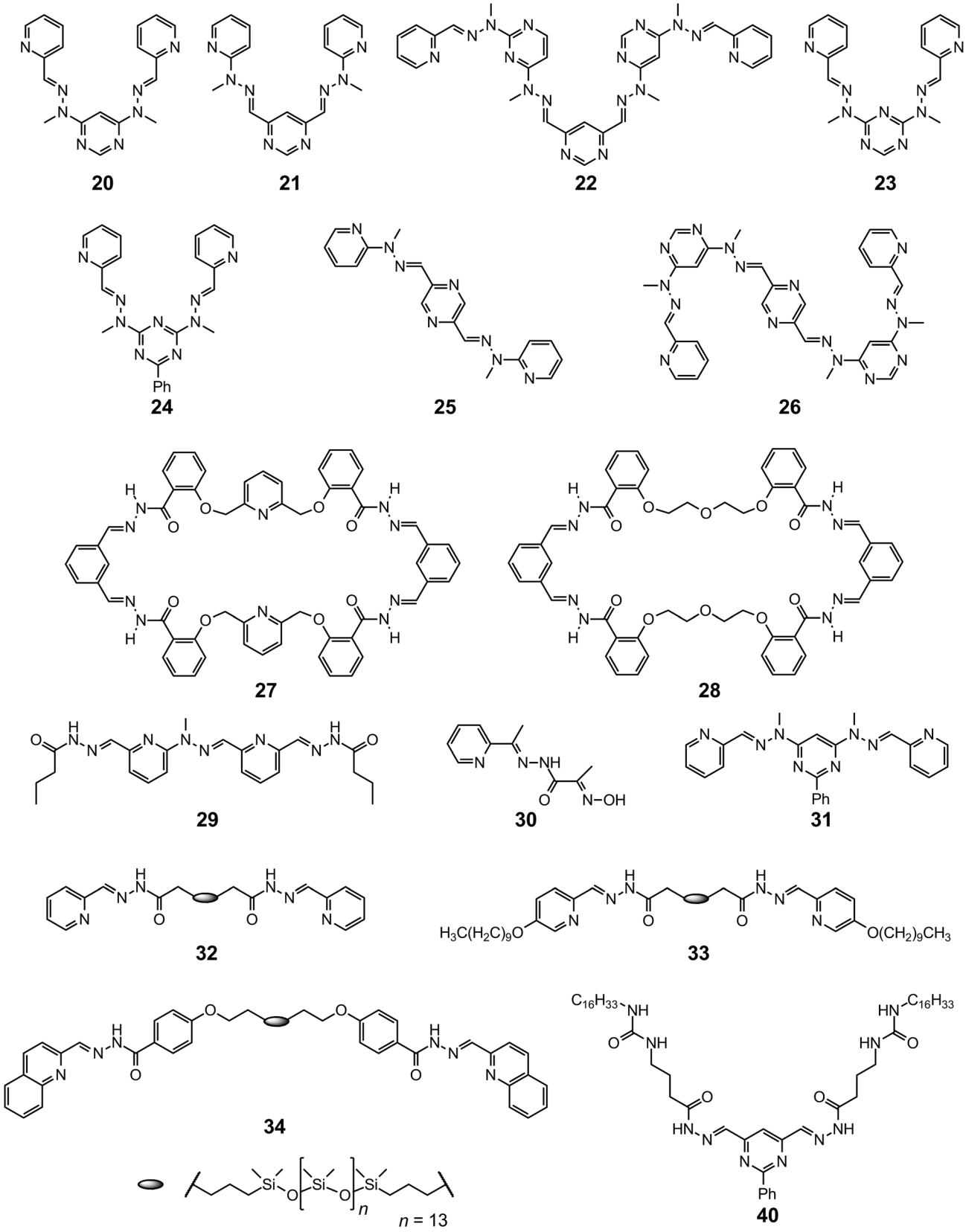

Scheme 12 Structures of hydrazone ligands used in metallo-assemblies.

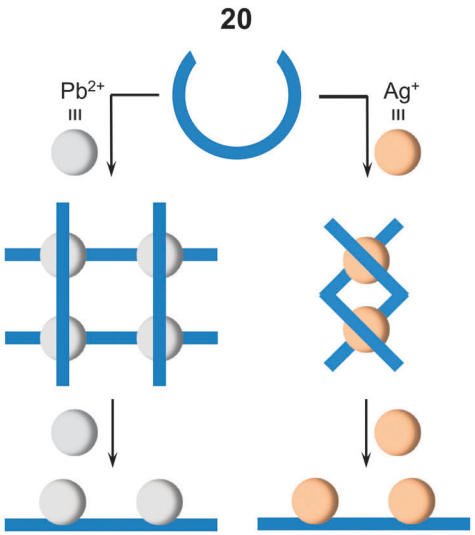

Fig. 3 Ligand **20** forms various stoichiometry-dependent metallo-assemblies.

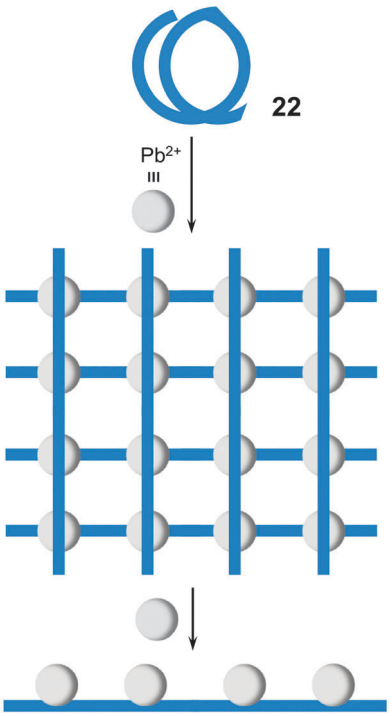

Fig. 4 Stoichiometry-controlled motional shape adaption in **22**.

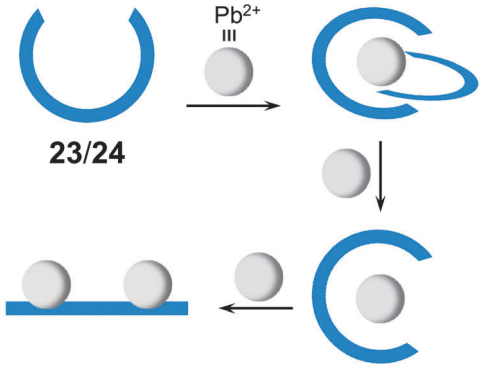

Fig. 5 Stoichiometry-controlled three-stage complex conversion in **23** and **24**.

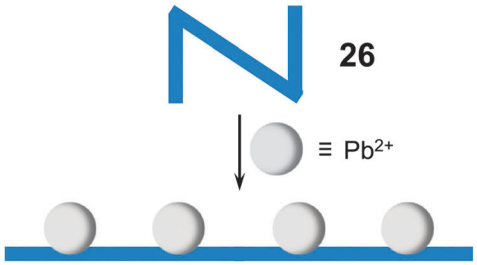

Fig. 6 "Twirling" motion in **26** upon coordination to Pb^{2+}.

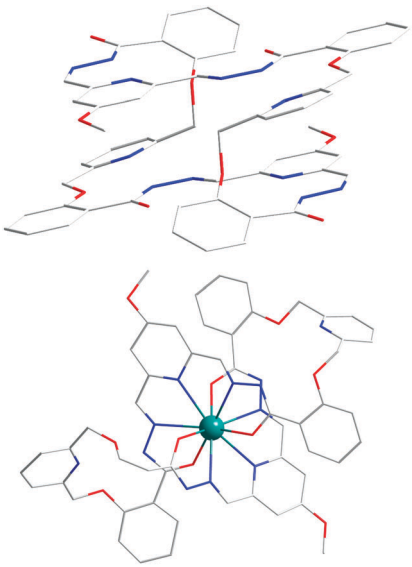

Fig. 7 The crystal structures of **27** (top) and the complex $[Eu\mathbf{27}]^{3+}$ (bottom).

Ligand **30**[46] possesses a terminal oxime group, in addition to the NNNO coordination site common for acylhydrazone ligands, and forms a dodecanuclear $3 \times [2 \times 2]$ grid with Ni^{2+}. The three $[2 \times 2]$ grids are fused together through a total of six deprotonated μ-(N,O) oxime bridges from three pairs of orthogonal units of **30** (Fig. 9).

3.2 Stimuli-induced structural interconversion

The structural interconversion between metallogrids and other forms of supramolecular assemblies takes advantage of the structural flexibility of the hydrazone ligands and the tunable coordination modes of the metal centers. For instance, ligands **23**[47] and **24**[41] are triazine-based bis-hydrazones that can host metal cations in linear or "U"-shaped conformations (Fig. 10). When dissolved in nitromethane (CH_3NO_2), **23** and **24** assemble with cobalt(II) tetrafluoroborate ($Co(BF_4)_2$) into $[2 \times 2]$ grids

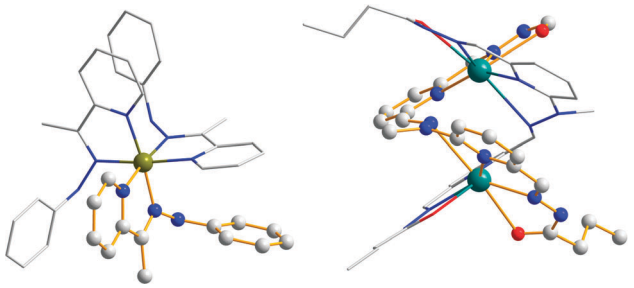

Fig. 8 The crystal structures of $[Fe\mathbf{4}_3]^{2+}$ (*fac*-Λ isomer) and $[Hg_2\mathbf{29}_2]^{4+}$ (left-handed form, right).

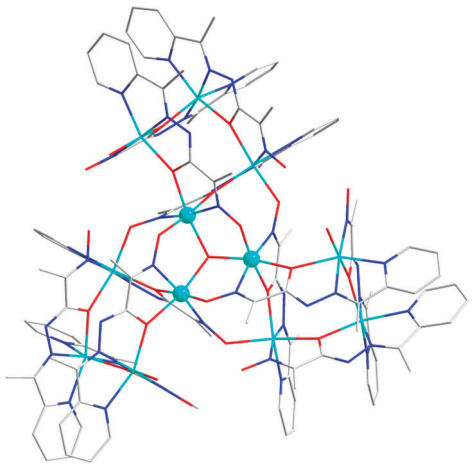

Fig. 9 The crystal structure of the 3 × [2 × 2] grid formed by **30** and Ni^{2+}.

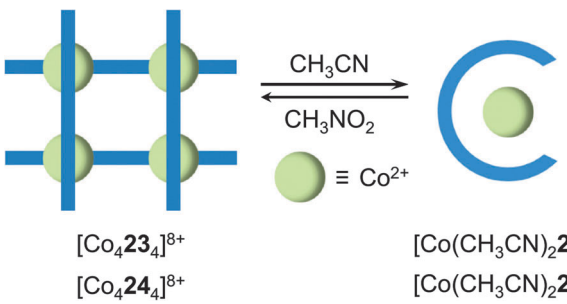

Fig. 10 The solvent induced dynamic interconversion between [2 × 2] grids and pincers.

($[Co_4\mathbf{23}_4]^{8+}$ and $[Co_4\mathbf{24}_4]^{8+}$) in which **23** and **24** extend their skeletons in a linear shape. Upon switching the solvent from CH_3NO_2 to CH_3CN, the grids convert into mononuclear helical pincer complexes ($[Co(CH_3CN)_2\mathbf{23}]^{2+}$ and $[Co(CH_3CN)_2\mathbf{24}]^{2+}$) where **23** and **24** contract to adopt a "U" shape.

Ligand **31**,[48] on the other hand, can form a tetranuclear [2 × 2] metallogrid $[Cu_4\mathbf{31}_4]^{8+}$ and a double helicate $[Cu_2\mathbf{31}_2]^{2+}$ with copper(II) triflate ($Cu(CF_3SO_3)_2$) and copper(I) triflate ($Cu(CD_3CN)_4CF_3SO_3$), respectively, as a result of the difference in the coordination modes of Cu^{2+} and Cu^+ (Fig. 11). The dynamic conversion of $[Cu_4\mathbf{31}_4]^{8+}$ into $[Cu_2\mathbf{31}_2]^{2+}$ is achieved by reduction with ascorbic acid in the presence of triflic acid

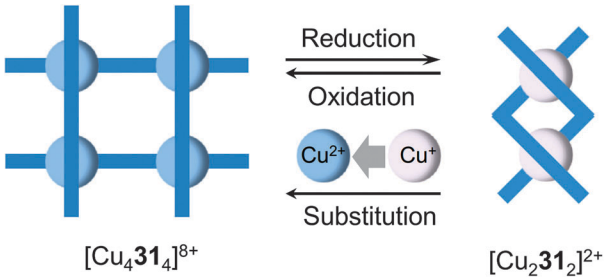

Fig. 11 The reversible transformation between the [2 × 2] metallogrid $[Cu_4\mathbf{31}_4]^{8+}$ and the double helicate $[Cu_2\mathbf{31}_2]^{2+}$.

(CF_3SO_3H) followed by neutralization with Et_3N. Alternatively, $[Cu_2\mathbf{31}_2]^{2+}$ can be transformed into $[Cu_4\mathbf{31}_4]^{8+}$ by either aerobic oxidation during crystallization or the substitution of Cu^{2+} with Cu^+.

3.3 Polymers and gels

The versatility of the hydrazone ligands enables their use in advanced applications as well, such as metallosupramolecular polymers and gels. A series of ditopic acylhydrazone ligands (**32–34**) featuring oligo-dimethylsilanoxyl-based spacers were used as monomers for preparing linear coordination polymers with Ni^{2+} and Zn^{2+}.[49] A simultaneous deprotonation occurs when two hydrazone NNO sites bind the metal cations, leading to the formation of neutral polymers (**35–38**, Scheme 13), with

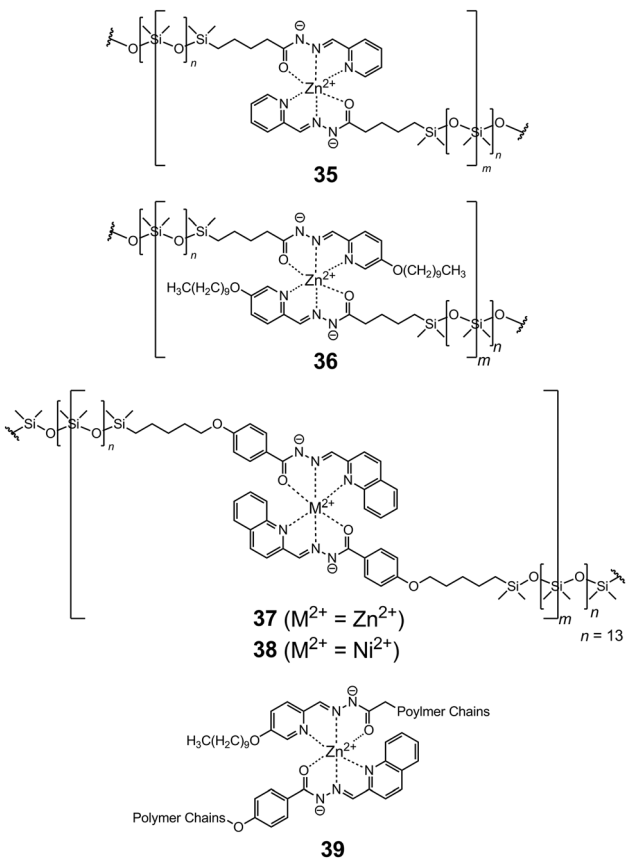

Scheme 13 The structures of neutral metallo-polymers **35–38**.

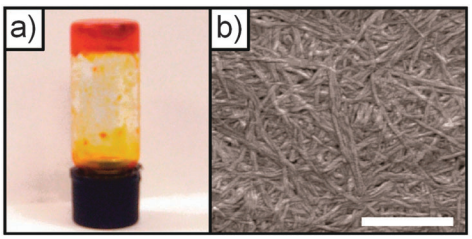

Fig. 12 (a) Photograph of the metallo-supramolecular polymer organogel formed by $[Zn_4\mathbf{40}_4]^{8+}$ at 20 mg ml^{-1} in toluene, and (b) the SEM image of a dried sample of the organogel (scale bar represents 1000 nm). Reproduced from ref. 52 with permission from the Centre National de la Recherche Scientifique (CNRS) and The Royal Society of Chemistry.

average molecular weights ranging from 15 000 to 45 000 g mol^{-1}. While **36** is obtained as a polymeric gum, **35**, **37** and **38** give transparent free-standing films. The Zn^{2+}-based polymers (**35**–**37**) are fluorescent whereas the Ni^{2+}-based **38** is nonfluorescent, possibly as a result of quenching by Ni^{2+}.

Given the reversibility of the coordination connectivity, homopolymers can be used for preparing polymer blends by dynamic exchange. For example, when stacks of **36** and **37** in the form of neat films are heated to 50 °C for 24 h, the constitutional metal–ligand exchange between **36** and **37** yields the heteropolymer **39**. This dynamic process opens up a new approach towards the construction of metallodynamers with tunable mechanical and optical properties,[50] as compared to their covalently built counterparts.[51]

The introduction of long urea side chains to the 4,6-disubstituted pyrimidyl-based bis-acylhydraone skeleton leads to precursor **40**,[52] which can form a [2 × 2] metallogrid gelator $[Zn_4\mathbf{40}_4]^{8+}$ upon coordination with Zn^{2+}. With a minimum concentration of gelation (MCG) of 18 mg ml^{-1} in toluene at room temperature, $[Zn_4\mathbf{40}_4]^{8+}$ forms organogels from the fibrillar network of metallogrid-based polymers (Fig. 12). This approach results in neutral organometallogels that are not affected by counterion effects, and can lead to [2 × 2] metallogrids with potentially interesting optical, electronic and magnetic properties.

4 Sensing applications

The broad range of the chemical and supramolecular reactivities of the hydrazone functional groups (Fig. 1) enables their use in the detection of cations, anions and other species. Here we summarize several recent examples of the use of hydrazones in sensing applications.

4.1 Cation sensing

In 2006, Tong *et al.*[53] reported an "off–on" fluorescent chemosensor for Cu^{2+} based on a rhodamine B-based hydrazone (**41**). As a spirolactam, **41** is weakly fluorescent, and upon coordination with Cu^{2+}, the lactam C–N bond breaks and the complex $[Cu\mathbf{41}]^+$ is formed *via* coordination with the ONO binding site (Scheme 14). The ring opening reaction enhances the fluorescence emission of **41**, which enables the fluorescence sensing of Cu^{2+} at the submicromolar level in buffered aqueous solutions.

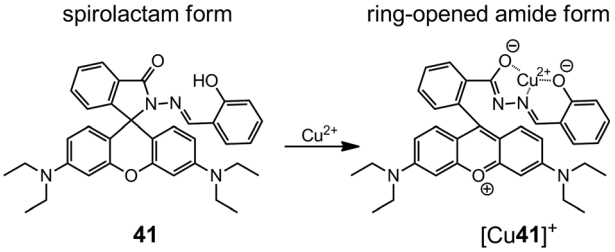

Scheme 14 The ring-opening reaction of **41** upon binding to Cu^{2+}.

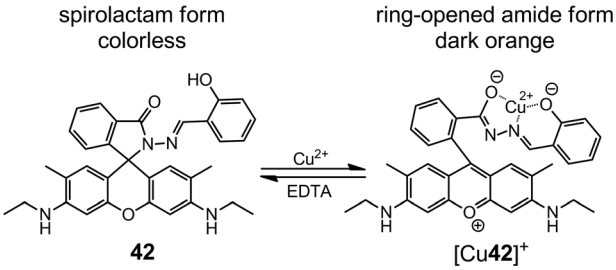

Scheme 15 The ring-opening reaction of **42** upon binding to Cu^{2+}.

The binding constant between **41** and Cu^{2+} is larger than 10^6 M^{-1} in Tris-HCl (10 mM, pH = 7.0) and water–CH_3CN (v/v = 1 : 1) buffer, which leads to a detection range between 25 nM and 3.3 μM, and high selectivity against Fe^{3+}, Fe^{2+}, Zn^{2+}, Pb^{2+} and Hg^{2+}.

By replacing the rhodamine B group in **41** with a rhodamine 6G group (**42**), Tong *et al.*[54] enhanced the Cu^{2+} sensing performance in both absorptiometric and fluorometric methods (Scheme 15). In sodium acetate–acetic acid (10 mM, pH = 7.0) water–ethanol (v/v = 1 : 1) buffer, **42** offers a limit of detection (LoD) of 10 nM with a linear range of 0.05–5.00 μM in the absorptiometric method, whereas in the fluorometric one it has a LoD of 25 nM with a linear range of 0.1–3.6 μM.

When the chromic group is changed to fluorescein (**43**),[55] the absorption profile of **43** becomes pH-dependent because of the two phenolic groups in the fluorescein unit (Scheme 16).

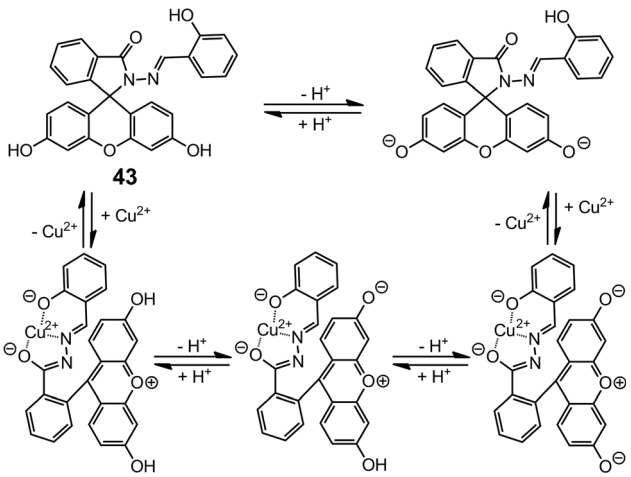

Scheme 16 The ring-opening reaction of **43** upon binding to Cu^{2+}, and the different products obtained at various pH values.

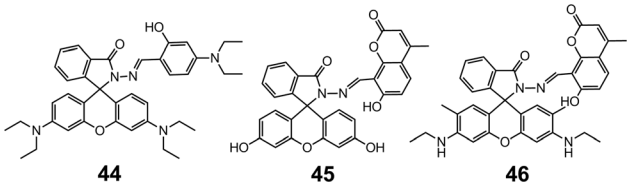

Scheme 17 The structures of hydrazones **44–46**.

Therefore, **43** can behave as a colorimetric YES and INHIBIT logic gate that can be modulated by both the concentration of Cu^{2+} and pH.

The lactam ring-opening reaction in rhodamine-derived hydrazones has since gained enormous popularity in the development of optical sensors for metal cations. The coordination strength of the hydrazones can be tuned by changing the aldehydes or ketones used in the condensation with the rhodamine hydrazides. For instance, **44**[56] is prepared by the condensation between rhodamine B hydrazide and 4-*N*,*N*-diethylaminosalicylaldehyde, instead of salicylaldehyde (**41**), which switches the selectivity of the metal from Cu^{2+} to Zn^{2+}. By forming a 1 : 1 complex with Zn^{2+}, **44** is able to detect Zn^{2+} in the concentration range of 0–10.0 μM with an LoD of 0.05 μM in HEPES (10 mM, pH = 7.0) water–ethanol (v/v = 1 : 9) buffer. The selectivity towards Zn^{2+} and sensing capability can be further enhanced by combining fluorescein hydrazide and 8-formyl-7-hydroxyl-4-methylcoumarin (**45**),[57] which leads to a LoD of 15 nM (Scheme 17).

Interestingly, when the fluorescein group in **45** is replaced by a rhodamine 6G group (**46**),[58] the system becomes highly selective for Ca^{2+} over other alkali-, alkaline earth- and transition metal cations. The binding with Ca^{2+} is accompanied by a 64-fold increase in fluorescence, leading to a LoD of 0.75 μM, and a linear working concentration range of 20–60 μM (Scheme 17).

The substitution of the phenol group in **42** with electron-donating (methyl, **47**) and electron-withdrawing (dicyano, **48**) allylic groups[59,60] leads to sensors having great affinity towards Pd^{2+} cation. The coordination proceeds with 2 : 1 stoichiometry through a similar spirolactam ring opening process. As fluorometric sensors, **47** and **48** have LoDs of 1.80×10^{-7} and 1.70×10^{-6} M, repsectively, and excellent selectivity for Pd^{2+} over a variety of metal cations, especially other platinum-group elements (PGEs), such as Pt^{2+}, Ru^{3+} and Rh^{3+}.

By introducing weak field ligands such as thiol and carboxylate groups, spirolactam-based hydrazones can effectively bind with the soft metal cation Hg^{2+}. Yang and Xu *et al.*[61] reported the sensing of Hg^{2+} with **49**, which was obtained from 2-furaldehyde and thiooxorhodamine B hydrazide. The fluorescence of **49** shows a 120-fold enhancement upon binding to Hg^{2+}, which proceeds in 2 : 1 stoichiometry in sodium acetate–acetic acid (pH = 7.0) water–DMF (v/v = 1 : 1) buffer with a detection range of 0.1–1 μM. Sensor **49** was also used for the *in vitro* Hg^{2+} fluorescence imaging in Rat Schwann cells (Fig. 13), showing the efficacy of these systems in biological applications (Scheme 18).

Park and Yoon *et al.*[62] prepared hydrazones **50** and **51** through the condensation of rhodamine B hydrazide with

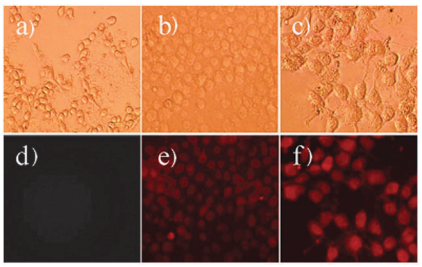

Fig. 13 Bright-field transmission images (a–c) and fluorescence images (d–e) of Rat Schwann cells incubated with 0 μM, 10 μM and 50 μM of Hg^{2+} ions for 30 min, respectively, in the presence of **49** (10 μM) upon excitation with green light. Reproduced from ref. 61.

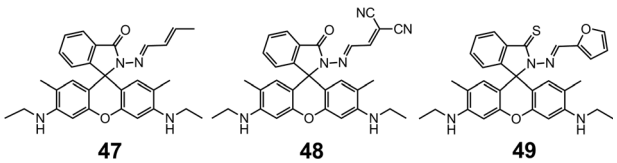

Scheme 18 The structures of hydrazones **47–49**.

2-mercaptobenzaldehyde and 2-carboxybenzaldehyde, respectively (Scheme 19). Compounds **50** and **51** form 2 : 1 and 1 : 1 complexes with Hg^{2+} in a water–CH_3CN (v/v = 99 : 1) mixture, respectively, with their corresponding LoDs being 1 and 4.2 nM, respectively. Moreover, both **50** and **51** were used in the *in vivo* imaging of nanomolar quantities of Hg^{2+} in the nematode *Caenorhabditis elegans* using fluorescence microscopy.

Simple hydrazones can also bind to metals through their NNN or NNO binding sites. For example, 2-pyridylhydrazone **52**[63] forms a stable 1 : 1 complex with Pd^{2+} (Fig. 14) with an association constant of 5.5×10^4 M^{-1} in methanol. Upon binding with Pd^{2+}, a drastic color change from yellow to red can be observed

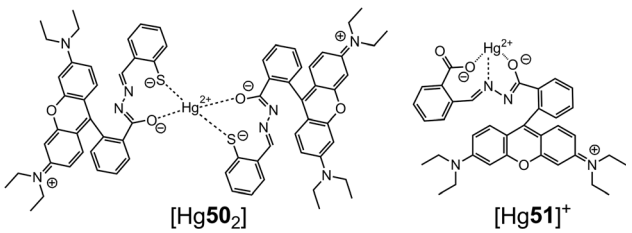

Scheme 19 The binding modes of hydrazones **50** and **51** with Hg^{2+}, respectively.

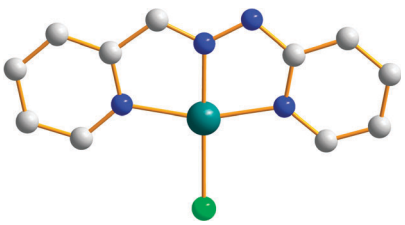

Fig. 14 The crystal structure of the complex [Pd**52**Cl].

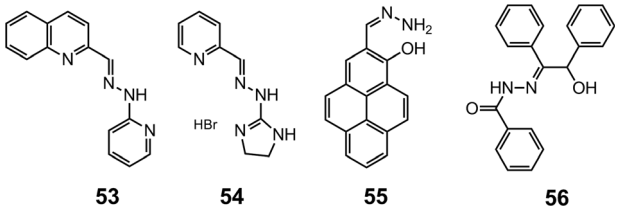

Scheme 20 The structures of hydrazones **53–56**.

by the naked eye, originating from the π–π* transitions in the complex $[Pd\mathbf{52}]^{2+}$.

Hydrazone **53** is obtained by replacing the pyridine-2-carboxaldehyde in **52** with quinoline-2-carboxaldehyde, which acts as a fluorescence emitter.[64] In alkaline methanol, the fluorescence of **53** can be quenched by Pd^{2+} in a ratiometric manner, making it a fluorescence "on–off" sensor for Pd^{2+}. The coupling between 2-imidazolyl hydrazine and pyridine-2-carboxaldehyde leads to **54**,[65] which selectively binds Cu^{2+} through the imine, pyridyl and imidazolyl nitrogens. Sensor **54** can be used in detecting 2.0–20 μM of Cu^{2+} in a water–methanol (v/v = 99 : 1) mixture (Scheme 20).

The simple non-substituted hydrazone **55**[66] is built on a pyrene fluorophore and can bind Zn^{2+} with its NNO binding site. Upon the formation of $[Zn\mathbf{55}]^{2+}$, the fluorescence is drastically enhanced because the photo-induced electron transfer (PET) from the hydrazone nitrogen to pyrene is blocked. Compound **55** is able to detect intracellular Zn^{2+} at the micromolar level in HaCaT and pancreatic β cells *in vitro*.

Acylhydrazones offer another NNO or ONO binding motif for metals. Hydrazone **56**[67] can be fabricated into microelectrodes with polyvinyl chloride (PVC) support for Er^{3+} sensing. This ion-selective electrode can achieve Er^{3+} detection in the range of 1.0 mM–0.3 nM with a LoD of 0.2 nM within the pH range of 3.0–9.0 using potentiometic methods.

Yang *et al.*[69] reported the ratiometric detection of Cu^{2+} with **57**, which has an ONO binding site (Fig. 15). Fluorescence quenching measurements show that **57** is able to selectively sense Cu^{2+} at 1 μM level in CH_3CN through photo-induced metal-to-ligand electron/energy transfer. The sensitivity of acylhydrazone-based Cu^{2+} sensors can be improved by integrating the mono ligand into a triphenylamine scaffold (**58**).[68] Compound **58** can form a 1 : 3 complex with Cu^{2+} through each

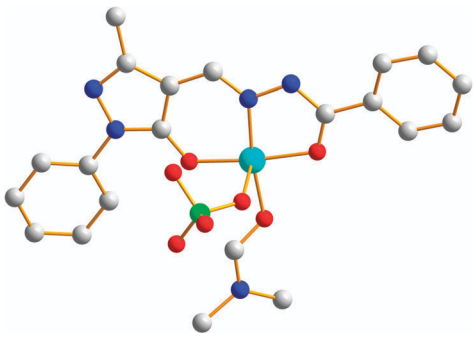

Fig. 15 The crystal structure of the complex $[Cu\mathbf{57}(DMF)ClO_4]$.

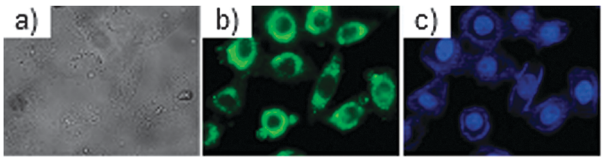

Fig. 16 (a) Bright-field transmission image of HeLa cells; (b) fluorescence images of Cu^{2+} in HeLa cells incubated with **58** (1 μM), and (c) when stained with Hoechst 33342. Reproduced from ref. 68.

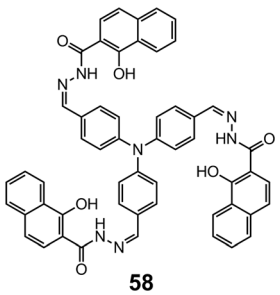

Scheme 21 The structure of hydrazone **58**.

of the three NOO binding sites. The fluorescence of **58** suffers drastic quenching when bound to Cu^{2+} because of the reverse PET process from the triphenylamine to the electron-deficient hydrazone nitrogens and phenolic oxygens. With an LoD for Cu^{2+} of 9.4 nM in a water–CH_3CN (v/v = 7 : 3) mixture, **58** can be used for the fluorescence imaging of micromolar amounts of Cu^{2+} in HeLa cells with low cytotoxicity (Fig. 16) (Scheme 21).

The introduction of pyrazinyl (**59**, Scheme 22)[70] and quinoxalinyl (**60**, Scheme 22)[71] groups into the hydrazones has led to the development of highly selective and sensitive sensors for Al^{3+} and Ni^{2+}, respectively. While compound **59** is able to detect Al^{3+} at the submicromolar level, compound **60** has a LoD of 1.47 μM for Ni^{2+}.

Tweezer-type[72] hydrazones **61**[73] and **62**[74] (Scheme 23) have also been developed as fluorescence "turn-on" cation sensors, by taking advantage of the restriction of the C=N bond rotation, which otherwise contributes to non-radiative decay. For instance, in the presence of Zn^{2+}, **61**[73] experiences a 49-fold increase in quantum yield, and this occurs with great selectivity especially over Cd^{2+}. Similarly, **62**[74] exhibits a 250-fold increase in quantum yield upon binding to Al^{3+}, providing a LoD of 0.77 μM in a water–methanol (v/v = 1 : 1) solution.

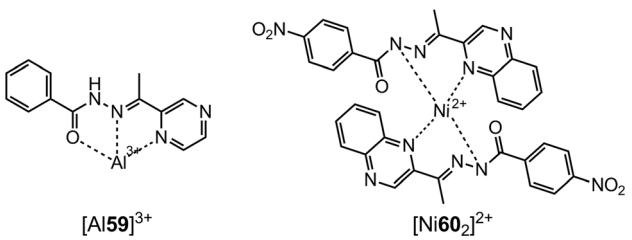

Scheme 22 The binding modes of hydrazones **59** and **60** with Al^{3+} and Ni^{2+}, respectively.

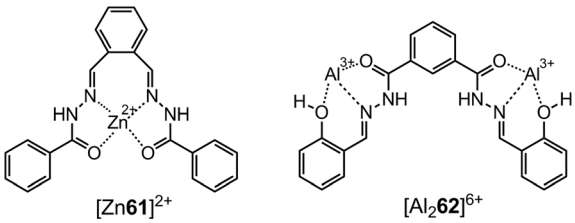

Scheme 23 The binding modes of hydrazones **61** and **62** with Zn^{2+} and Al^{3+}, respectively.

4.2 Anion sensing

The acidic nature of the hydrazone N–H group allows for the detection of anionic species through H-bond interactions that alter the photophysical properties of the system. These spectroscopic changes make hydrazones ideal for anion sensing applications, especially for the fluoride anion.[75–77] Fluoride usually forms H-bonded adducts [R–N–H···F^-] with hydrazones, and in certain cases, the interaction between the anion and the hydrazone N–H proton is so strong that deprotonation occurs, leading to the formation of HF_2^- species, and further enhancement of the photophysical changes. For example, the indole-derived hydrazone **63**[78] can form a 1 : 1 complex **63**···$\mathbf{F}^-$ in the presence of less than 2 equiv. of F^-, above which the hydrazone N–H is deprotonated (Scheme 24). The association with F^- causes a red-shift and an increase in the UV-vis absorption and fluorescence emission of **63**, respectively. This property makes **63** a dual-channel fluoride receptor. Similarly, hydrazone **64**[79] has a reduced HOMO–LUMO gap in its fluoride complex **64**···$\mathbf{F}^-$, which gives rise to a large red-shift to the near IR region in its UV-vis absorption spectrum (Scheme 25).

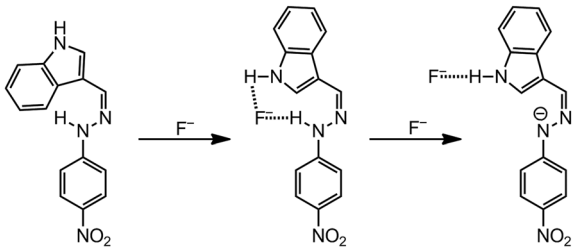

Scheme 24 The reaction between **63** and F^-.

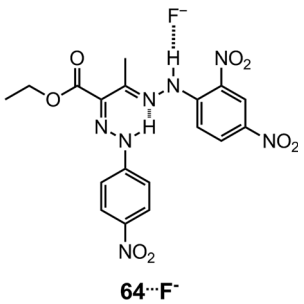

Scheme 25 The structure of the **64**···$\mathbf{F}^-$ adduct.

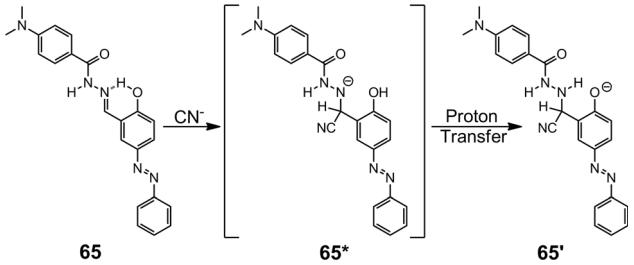

Scheme 26 The nucleophilic addition of CN^- to **65**.

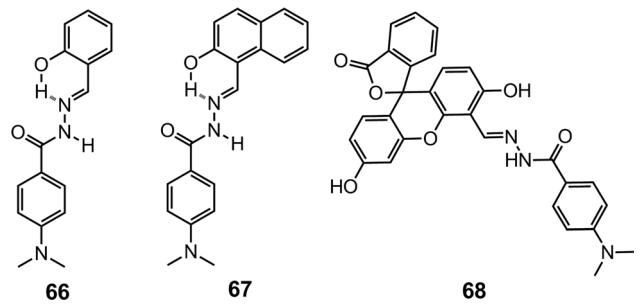

Scheme 27 The structures of hydrazones **66–68**.

This hydrazone is a sensitive sensor for F^-, and allows for the "naked-eye" detection of the anion at levels as low as 50 ppm in toothpaste solution samples.

The imine (C=N) bond in hydrazones can be susceptible to nucleophilic attack, especially by cyanide (CN^-), making these systems good candidates for reaction-based sensing.[16a,c] For instance,[80] the addition of CN^- to the imine group of **65** converts it into a disubstituted hydrazine species **65′** through a proton transfer (Scheme 26). This transformation gives rise to a new absorption peak at 525 nm, which is responsible for the drastic color change of the solution from faint yellow to dark red. Qualified as a "naked-eye" CN^- sensor, **65** is capable of detecting submillimolar CN^- with a LoD of 1.5 μM in a water–DMSO (v/v = 1 : 1) solution.

When a fluorophore is present in conjugation with the hydrazone system, such as in **66** and **67**,[81] the fluorescence is usually quenched as a result of excited state charge transfer (ESCT). The nucleophilic addition of CN^- can effectively disrupt the ESCT process in **66** and **67**, leading to remarkable fluorescence recovery. In this way, compounds **66** and **67** are capable of detecting submicromolar quantities of CN^- with LoDs at the 10 nM level (Scheme 27).

The addition of CN^- can also be used in turning on the fluorescence resonance energy transfer (FRET) in hydrazones containing energy donor–acceptor pairs. The energy donor 4-(*N*,*N*-dimethylamino)benzamide and the energy acceptor fluorescein are connected by a hydrazone linkage in **68**,[82] where FRET is suppressed since fluorescein exists in the closed, non-fluorescent spirolactam form. Upon reaction with CN^-, fluorescein undergoes ring opening and becomes fluorescent, which turns on the FRET process. As a two-channel fluorescence sensor for CN^-, **68** works in the CN^- concentration range

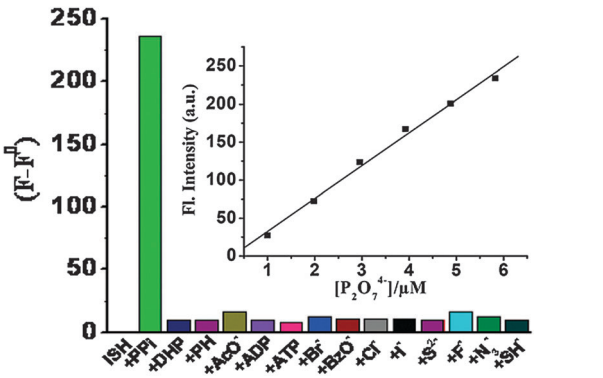

Fig. 17 Changes in fluorescence intensity (monitored at 508 nm) of $[Al\mathbf{62}]^{3+}$ after the addition of 2.0 equiv. of each anion in water–methanol (v/v = 1 : 1, pH = 7.5). Inset shows the fluoresence intensity *vs.* the concentration of PPi. Reproduced from ref. 74.

of 0–90 μM, with a LoD of 0.44 μM in a water–DMF (v/v = 1 : 9) solution.

Metal–hydrazone complexes have been developed as anion sensors as well, by taking advantage of anion–metal interactions. The fluorescent Al^{3+} complex of **62** reported by Goswami *et al.*[74] shows affinity towards pyrophosphate (PPi, $P_2O_7^{4-}$) *via* Al^{3+}–PPi interactions. The complex $[Al\mathbf{62}]^{3+}$ exhibits strong blue fluorescence that is quenched upon the addition of PPi (Fig. 17). This process provides a LoD of 1.7 μM for PPi with great discrimination over common anions, especially adenosine diphosphate (ADP) and triphosphate (ATP).

The Zn^{2+} complex of the naphthol-based symmetric acylhydrazone **69**[83] is weakly emissive (Scheme 28); however, upon coordination with PPi, the fluorescence intensity increases and is accompanied by a color change from colorless to yellow in HEPES (20 mM, pH = 7.4) buffer. With a LoD of 0.16 μM, the complex $[Zn\mathbf{69}]^{2+}$ is used as a PPi-specific fluorescent probe for DNA pyrosequencing, and is able to detect trace amounts of PPi from DNA polymerase chain reactions even in the presence of large excess of ATP (Fig. 18).

The fluorescence quantum yield (Φ_F) of acylhydrazone **70**,[84] which is functionalized with a BODIPY fluorophore, drops from 0.27 to 0.038 when forming a 1 : 1 complex with Zn^{2+} ($[Zn\mathbf{70}]^{2+}$). Nonetheless, this complex can be used in detecting PPi and ATP with micromolar LoDs of 1.0 and 2.4 μM, respectively, which is below their normal biological concentrations (Scheme 28).

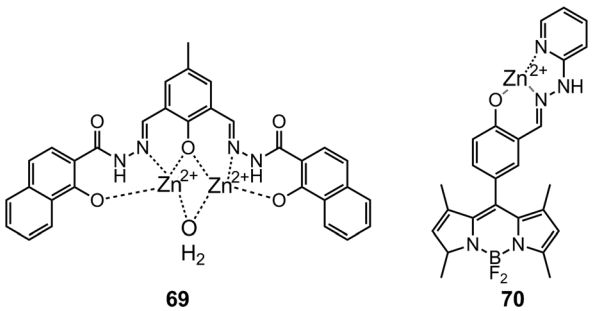

69 70

Scheme 28 The structures of Zn^{2+}–hydrazone complexes $[Zn\mathbf{69}]^{2+}$ and $[Zn\mathbf{70}]^{2+}$.

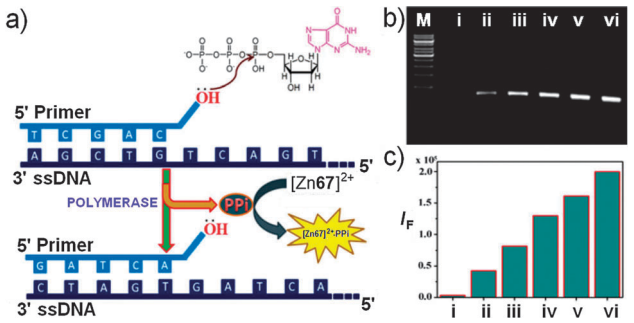

Fig. 18 (a) Mechanism of sensing PPi released from PCR by $[Zn\mathbf{69}]^{2+}$; (b) gel electrophoresis of finished PCR mixtures (M = DNA marker). (c) Fluorescence intensity of the sensor $[Zn\mathbf{69}]^{2+}$ at 525 nm upon addition of the finished PCR product mixture. (i) 10 μM of the finished PCR product mixture performed without template DNA; 10 μM of the finished PCR product mixture performed with template DNA after (ii) 29 cycles, (iii) 30 cycles, (iv) 31 cycles, (v) 32 cycles, and (vi) 35 cycles. Reprinted with permission from S. Anbu, S. Kamalraj, C. Jayabaskaran and P. S. Mukherjee, *Inorg. Chem.*, 2013, **52**, 8294–8296. Copyright 2013 American Chemical Society.

4.3 Other sensing applications

Trishydrazones **71–73**[85] are C_3-symmetric compounds with planar cores stabilized by peripheral intramolecular H-bonds. The structural distortion caused by the steric hindrance between the peripheral substituents can lower the degree of overall π-conjugation, and hence a blue shift is observed for these systems as crowdedness increases from **71** to **73**. Similar changes can occur when the intramolecular H-bonding is disrupted, hence compounds **71–73** are spectroscopically responsive towards H-bond acceptors. For instance, when a thin film of **71** is exposed to vapors of volatile primary and secondary amines, it undergoes a fast color change from pink to dark-orange as a result of conformational switching. Using this sensing mechanism Lee *et al.* have demonstrated the "naked-eye" sensing of volatile amines (Scheme 29).

The intrinsic characteristics of the hydrazone group has allowed its use in bifunctional sensing applications as well. For example, the 4,6-naphthalimide-based hydrazone **74**[86] emits green fluorescence in CH_3CN, which is completely quenched upon complexation with Cu^{2+}. The same effect is observed with F^-, which can effectively deprotonate the hydrazone N–H group, leading to quenching. Therefore, **74** can be used as a bifunctional "turn-off" chemosensor for sensing either Cu^{2+} or F^- at micromolar levels (Scheme 30).

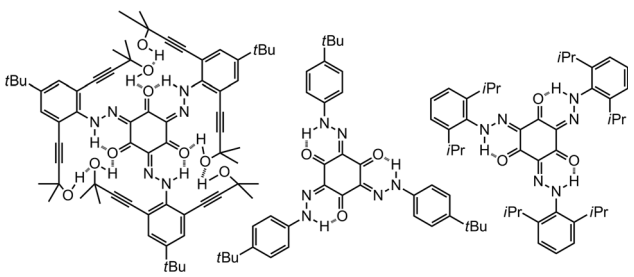

71 72 73

Scheme 29 The structures of trishydrazones **71–73**.

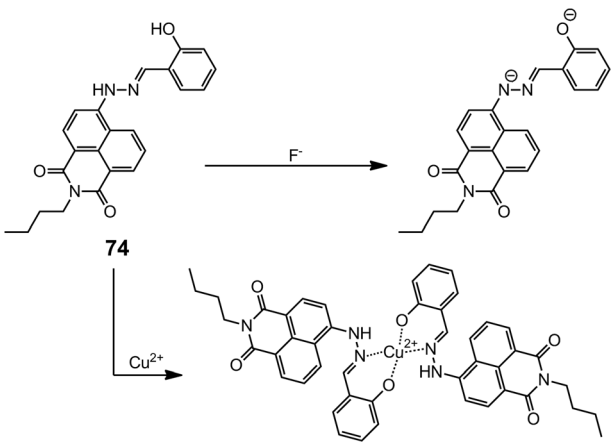

Scheme 30 The bifunctional sensing of Cu^{2+} and F^- with **74**.

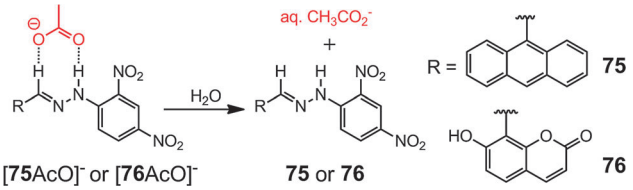

Scheme 31 The sensing of water with $[\mathbf{75}AcO]^-$ and $[\mathbf{76}AcO]^-$.

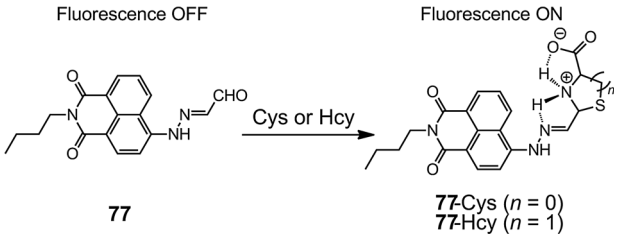

Scheme 32 The sensing of Cys and Hcy with **77** by restricting the C=N bond rotation.

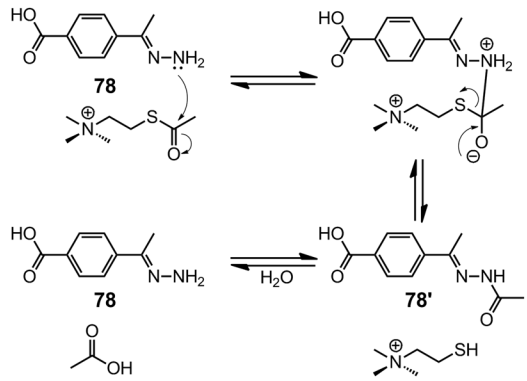

Scheme 33 Mechanism for the hydrolysis of ATCh by the AChE mimic **78**.

Acetate (AcO^-) effectively binds with hydrazones mainly through H-bonding, the breaking of which can be used to quantify the disruptive additive. Chang *et al.*[87] reported the detection of water in organic solvents using the hydrazone–acetate complexes $[\mathbf{75}AcO]^-$ and $[\mathbf{76}AcO]^-$. Both complexes undergo color changes from red to yellow, indicating the breaking of the hydrazone–acetate interaction, as a result of the formation of the more favored aqueous acetate species (Scheme 31). While $[\mathbf{75}AcO]^-$ provides a LoD as low as 0.071% for water in THF, $[\mathbf{76}AcO]^-$ has a LoD of 0.12% for water in CH_3CN.

Similarly, hydrazone–cation complexes can be used for the sensing of metallophilic species. Complex $[Cu\mathbf{41}]^+$ (Scheme 14),[88] formed during the detection of Cu^{2+}, is a weakly fluorescent species because of the fluorescence inner filter effect (IFE). Upon the addition of Cys, IFE is halted as a result of the dissociation of $[Cu\mathbf{41}]^+$, leading to emission turn-on that can be used in the detection of micromolar Cys with a LoD of 0.17 μM. Although $[Cu\mathbf{41}]^+$ shows great selectivity for Cys over a variety of amino acids, it cannot differentiate Cys from other thiol-based molecules, such as homocysteine (Hcy) and glutathione.

In analogy to some fluorescence "turn-on" hydrazone-based metal sensors (Scheme 22), fluorescence enhancement by restricting C=N bond rotation can also be used for Cys or Hcy detection.[89] The fluorescence from the naphthalimide group in **77** is quenched by the $E \leftrightharpoons Z$ isomerization of the C=N bond. Upon treatment with Cys and Hcy, thiazolidine and thiazinane derivatives are formed, respectively, through the cyclization reaction with the aldehyde group in **75** (Scheme 32). Therefore, the Φ_F of **77** increases from 0.012 to 0.625, as the C=N isomerization in **77** is restricted by intramolecular H-bonding between the positively charged thiazolidine or thiazinane N–H proton and the imine nitrogen. Compound **77** has been used for the *in vitro* detection of submillimolar Cys in both buffer solutions and *Tetrahymena thermophila* cells.

Machado *et al.*[90] reported the hydrolysis of acetylthiochiline (ATCh) by the unsubstituted hydrazone **78**. This process provides a ratiometric electrochemical response to the concentration of ATCh, making it an acetylcholinesterase (AChE) mimic. Compound **78** first forms a supramolecular complex with ATCh through cation–π interaction, followed by a nucleophilic attack on the carbonyl group by the hydrazone nitrogen, forming the acylhydrazone **78′** that is prone to hydrolysis (Scheme 33). Differential pulse voltammetry reveals a linear response of the current to the concentration of ATCh in the presence of **78**, which allows for its detection in the millimolar to submillimolar range with a LoD of 20 μM.

5 Concluding remarks

For some time now hydrazones have been bundled under the imine banner,[91] because of the similarities between both functional groups. This point is made evident by the scarcity of focused reviews and/or monographs dealing with only hydrazone chemistry, in spite of its vast richness and popularity. In this review we aimed at showcasing the uniqueness of hydrazones in the context of supramolecular chemistry, albeit it is clear to us that this functional group is important and pervasive in other fields as well. There are a number of factors

that distinguish the hydrazone functional group from its imine counterpart, namely: (i) the stability of the C=N double bond to hydrolysis under neutral conditions because of a mesomeric effect; (ii) the existence of an extra amino-type nitrogen in the system that enhances this group's coordination capability; and (iii) the acidic N–H proton that can be utilized in intramolecular H-bonding, anion sensing and even coordination with metals. These qualities not only set this functional group apart from imines, but they also open up complementary research directions that are not easily accessible by the latter. We are hopeful that this review will lead to a divergence in thinking about hydrazones as only a subgroup of imines, and facilitate the exploration of its rich chemistry[92] as it relates to supramolecular chemistry and beyond.

Acknowledgements

We would like to thank Dartmouth College and the National Science Foundation CAREER program (CHE-1253385) for their generous support. We are also thankful to Prof. David S. Glueck for his input.

References

1 (*a*) M. Hidai and Y. Mizobe, *Chem. Rev.*, 1995, **95**, 1115–1133; (*b*) D. Enders, L. Wortmann and R. Peters, *Acc. Chem. Res.*, 2000, **33**, 157–169; (*c*) R. Lazny and A. Nodzewska, *Chem. Rev.*, 2010, **110**, 1386–1434; (*d*) S. Kobayashi, Y. Mori, J. S. Fossey and M. M. Salter, *Chem. Rev.*, 2011, **111**, 2626–2704.

2 (*a*) P. Vicini, F. Zani, P. Cozzini and I. Doytchinova, *Eur. J. Med. Chem.*, 2002, **37**, 553–564; (*b*) C. Loncle, J. Brunel, N. Vidal, M. Dherbomez and Y. Letourneux, *Eur. J. Med. Chem.*, 2004, **39**, 1067–1071; (*c*) L. Savini, L. Chiasserini, V. Travagli, C. Pellerano, E. Novellino, S. Cosentino and M. Pisano, *Eur. J. Med. Chem.*, 2004, **39**, 113–122; (*d*) M. Cocco, C. Congiu, V. Lilliu and V. Onnis, *Bioorg. Med. Chem.*, 2006, **14**, 366–372; (*e*) A. Masunari and L. C. Tavares, *Bioorg. Med. Chem.*, 2007, **15**, 4229–4236; (*f*) P. Vicini, M. Incerti, P. La Colla and R. Loddo, *Eur. J. Med. Chem.*, 2009, **44**, 1801–1807.

3 (*a*) J.-M. Lehn, *Chem. Soc. Rev.*, 2007, **36**, 151–160; (*b*) J.-M. Lehn, in *Topics in Current Chemistry*, ed. M. Barboiu, Springer, Berlin, 2012, vol. 322, book section Constitutional Dynamic Chemistry: Bridge from Supramolecular Chemistry to Adaptive Chemistry, pp. 1–32; (*c*) J.-M. Lehn, *Angew. Chem., Int. Ed.*, 2013, **52**, 2836–2850.

4 (*a*) F. J. Uribe-Romo, C. J. Doonan, H. Furukawa, K. Oisaki and O. M. Yaghi, *J. Am. Chem. Soc.*, 2011, **133**, 11478–11481; (*b*) D. N. Bunck and W. R. Dichtel, *J. Am. Chem. Soc.*, 2013, **135**, 14952–14955; (*c*) X.-P. Zhou, Y. Wu and D. Li, *J. Am. Chem. Soc.*, 2013, **135**, 16062–16065.

5 (*a*) S. Rowan, S. Cantrill, G. Cousins, J. Sanders and J. Stoddart, *Angew. Chem., Int. Ed.*, 2002, **41**, 898–952; (*b*) P. T. Corbett, J. Leclaire, L. Vial, K. R. West, J.-L. Wietor, J. K. M. Sanders and S. Otto, *Chem. Rev.*, 2006, **106**, 3652–3711; (*c*) Dynamic Combinatorial Chemistry, *Drug Discovery, Bioorganic Chemistry, and Materials Science*, ed. B. L. Miller, John Wiley and Sons, Hoboken, New Jersey, 2010; (*d*) Y. Jin, C. Yu, R. J. Denman and W. Zhang, *Chem. Soc. Rev.*, 2013, **42**, 6634–6654.

6 R. Raue, A. Brack and K. Lange, *Angew. Chem., Int. Ed. Engl.*, 1991, **30**, 1643–1644.

7 R. Lygaitis, V. Getautis and J. V. Grazulevicius, *Chem. Soc. Rev.*, 2008, **37**, 770–788.

8 C. Serbutoviez, C. Bosshard, G. Knopfle, P. Wyss, P. Pretre, P. Gunter, K. Schenk, E. Solari and G. Chapuis, *Chem. Mater.*, 1995, **7**, 1198–1206.

9 (*a*) F. R. Japp and F. Klingemann, *Ber. Dtsch. Chem. Ges.*, 1887, **20**, 2942–2944; (*b*) F. R. Japp and F. Klingemann, *Ber. Dtsch. Chem. Ges.*, 1887, **20**, 3284–3286; (*c*) F. R. Japp and F. Klingemann, *Ber. Dtsch. Chem. Ges.*, 1887, **20**, 3398–3401; (*d*) F. R. Japp and F. Klingemann, *Justus Liebigs Ann. Chem.*, 1888, **247**, 190–225.

10 A. C. Day and M. C. Whiting, *Org. Synth.*, 1988, **6**, 10–12.

11 G. Stork and J. Benaim, *Org. Synth.*, 1988, **6**, 242–244.

12 S. Wagaw, B. H. Yang and S. L. Buchwald, *J. Am. Chem. Soc.*, 1998, **120**, 6621–6622.

13 V. Lefebvre, T. Cailly, F. Fabis and S. Rault, *J. Org. Chem.*, 2010, **75**, 2730–2732.

14 (*a*) *Molecular Machines and Motors*, ed. J.-P. Sauvage, Springer, New York, 2001; (*b*) E. R. Kay, D. A. Leigh and F. Zerbetto, *Angew. Chem., Int. Ed.*, 2007, **46**, 72–191; (*c*) V. Balzani, A. Credi and M. Venturi, *Molecular Decices and Machines - Concepts and Perspectives for the Nanoworld*, Wiley-VCH, Weinheim, Germany, 2008; (*d*) M.-M. Russew and S. Hecht, *Adv. Mater.*, 2010, **22**, 3348–3360; (*e*) *Molecular Switches*, ed. B. L. Feringa, Wiley-VCH, Weinheim, Germany, 2nd edn, 2011; (*f*) A. Coskun, M. Banaszak, R. D. Astumian, J. F. Stoddart and B. A. Grzybowski, *Chem. Soc. Rev.*, 2012, **41**, 19–30; (*g*) A. C. Fahrenbach, S. C. Warren, J. T. Incorvati, A.-J. Avestro, J. C. Barnes, J. F. Stoddart and B. A. Grzybowski, *Adv. Mater.*, 2013, **25**, 331–348.

15 (*a*) M. Ruben, J.-M. Lehn and P. Müller, *Chem. Soc. Rev.*, 2006, **35**, 1056–1067; (*b*) J. G. Hardy, *Chem. Soc. Rev.*, 2013, **42**, 7881–7899.

16 (*a*) H. Miyaji and J. Sessler, *Angew. Chem., Int. Ed.*, 2001, **40**, 154–157; (*b*) E. V. Anslyn, *J. Org. Chem.*, 2007, **72**, 687–699; (*c*) D.-G. Cho and J. L. Sessler, *Chem. Soc. Rev.*, 2009, **38**, 1647–1662; (*d*) P. A. Gale, *Chem. Commun.*, 2011, **47**, 82–86; (*e*) M. T. Albelda, J. C. Frias, E. Garcia-Espana and H. J. Schneider, *Chem. Soc. Rev.*, 2012, **41**, 3859–3877; (*f*) M. Wenzel, J. R. Hiscock and P. A. Gale, *Chem. Soc. Rev.*, 2012, **41**, 480–520; (*g*) A. P. F. Turner, *Chem. Soc. Rev.*, 2013, **42**, 3148–3196; (*h*) P. A. Gale, N. Busschaert, C. J. E. Haynes, L. E. Karagiannidis and I. L. Kirby, *Chem. Soc. Rev.*, 2014, **43**, 205–241.

17 (*a*) H. C. Yao, *J. Org. Chem.*, 1964, **29**, 2959–2963; (*b*) J. C. Tobin, A. F. Hegarty and F. L. Scott, *J. Chem. Soc. B*, 1971, 2198–2202; (*c*) J. L. Wong and M. F. Zady, *J. Org. Chem.*, 1975, **40**, 2512–2516.

18 A. C. Pratt, *Chem. Soc. Rev.*, 1977, **6**, 63–81.

19 A. Padwa, *Chem. Rev.*, 1977, **77**, 37–68.

20 (*a*) P. Courtot, J. Le Saint and R. Pichon, *Bull. Soc. Chim. Fr.*, 1975, 2538–2542; (*b*) P. Courtot, R. Pichon and J. Le Saint, *Tetrahedron Lett.*, 1976, 1181–1184; (*c*) R. Pichon, J. Le Saint and P. Courtot, *Tetrahedron*, 1981, **37**, 1517–1524.
21 S. Yamamura, T. Tamaki, T. Seki, M. Sakuragi, Y. Kawanishi and K. Ichimura, *Chem. Lett.*, 1992, 543–546.
22 D. G. Belov, B. G. Rogachev, L. I. Tkachenko, V. A. Smirnov and S. M. Aldoshin, *Russ. Chem. Bull.*, 2000, **49**, 666–668.
23 Y. E. Semenov, V. A. Smirnov, S. M. Aldoshin and B. G. Rogachev, *Russ. Chem. Bull.*, 2001, **50**, 2471–2472.
24 M. N. Chaur, D. Collado and J.-M. Lehn, *Chem.–Eur. J.*, 2011, **17**, 248–258.
25 G. Vantomme and J.-M. Lehn, *Angew. Chem., Int. Ed.*, 2013, **52**, 3940–3943.
26 S. M. Landge and I. Aprahamian, *J. Am. Chem. Soc.*, 2009, **131**, 18269–18271.
27 S. M. Landge, E. Tkatchouk, D. Benítez, D. A. Lanfranchi, M. Elhabiri, W. A. Goddard III and I. Aprahamian, *J. Am. Chem. Soc.*, 2011, **133**, 9812–9823.
28 X. Su, T. Lessing and I. Aprahamian, *Beilstein J. Org. Chem.*, 2012, **8**, 872–876.
29 X. Su and I. Aprahamian, *Org. Lett.*, 2011, **13**, 30–33.
30 (*a*) T. Dudev and C. Lim, *Chem. Rev.*, 2003, **103**, 773–788; (*b*) D. E. Wilcox, *Inorg. Chim. Acta*, 2008, **361**, 857–867.
31 X. Su, T. F. Robbins and I. Aprahamian, *Angew. Chem., Int. Ed.*, 2011, **50**, 1841–1844.
32 D. Ray, J. T. Foy, R. P. Hughes and I. Aprahamian, *Nat. Chem.*, 2012, **4**, 757–762.
33 (*a*) K. Ichimura, *Chem. Rev.*, 2000, **100**, 1847–1873; (*b*) R. Eelkema and B. L. Feringa, *Org. Biomol. Chem.*, 2006, **4**, 3729–3745; (*c*) I. M. Saez and J. W. Goodby, in *Liquid Crystalline Functional Assemblies and Their Supramolecular Structures*, ed. T. Kato, Springer-Verlag Berlin, Heidelberger Platz 3, D-14197 Berlin, Germany, 2008, vol. 128, pp. 1–62; (*d*) *Liquid Crystal Beyond Displays: Chemistry, Physics, and Applications*, ed. Q. Li, Wiley-VCH, Weinheim, Germany, 2012; (*e*) Y. Wang and Q. Li, *Adv. Mater.*, 2012, **24**, 1926–1945.
34 X. Su, S. Voskian, R. P. Hughes and I. Aprahamian, *Angew. Chem., Int. Ed.*, 2013, **52**, 10734–10739.
35 A.-M. Stadler, N. Kyritsakas, R. Graff and J.-M. Lehn, *Chem.–Eur. J.*, 2006, **12**, 4503–4522.
36 A.-M. Stadler, N. Kyritsakas, G. Vanghan and J.-M. Lehn, *Chem.–Eur. J.*, 2007, **13**, 59–68.
37 D. J. Hutchinson, L. R. Hanton and S. C. Moratti, *Inorg. Chem.*, 2010, **49**, 5923–5934.
38 D. J. Hutchinson, L. R. Hanton and S. C. Moratti, *Inorg. Chem.*, 2011, **50**, 7637–7649.
39 D. J. Hutchinson, L. R. Hanton and S. C. Moratti, *Inorg. Chem.*, 2013, **52**, 2716–2728.
40 D. J. Hutchinson, S. A. Cameron, L. R. Hanton and S. C. Moratti, *Inorg. Chem.*, 2012, **51**, 5070–5081.
41 J. Ramírez, A.-M. Stadler, L. Brelot and J.-M. Lehn, *Tetrahedron*, 2008, **64**, 8402–8410.
42 A.-M. Stadler, J. Ramírez and J.-M. Lehn, *Chem.–Eur. J.*, 2010, **16**, 5369–5378.
43 J. M. Klein, J. K. Clegg, V. Saggiomo, L. Reck, U. Luning and J. K. M. Sanders, *Dalton Trans.*, 2012, **41**, 3780–3786.
44 C. P. Sebli, S. E. Howson, G. J. Clarkson and P. Scott, *Dalton Trans.*, 2010, **39**, 4447–4454.
45 G. Schaeffer, J. M. Harrowfield, J.-M. Lehn and A. K. H. Hirsch, *Polyhedron*, 2012, **41**, 40–43.
46 Y. S. Moroz, S. Demeshko, M. Haukka, A. Mokhir, U. Mitra, M. Stocker, P. Müller, F. Meyer and I. O. Fritsky, *Inorg. Chem.*, 2012, **51**, 7445–7447.
47 J. Ramírez, A.-M. Stadler, N. Kyritsakas and J.-M. Lehn, *Chem. Commun.*, 2007, 237–239.
48 A.-M. Stadler, C. Burg, J. Ramírez and J.-M. Lehn, *Chem. Commun.*, 2013, **49**, 5733–5735.
49 C.-F. Chow, S. Fujii and J.-M. Lehn, *Angew. Chem., Int. Ed.*, 2007, **46**, 5007–5010.
50 C. F. Chow, S. Fujii and J.-M. Lehn, *Chem.–Asian J.*, 2008, **3**, 1324–1335.
51 T. Ono, S. Fujii, T. Nobori and J.-M. Lehn, *Chem. Commun.*, 2007, 4360–4362.
52 J. G. Hardy, X.-Y. Cao, J. Harrowfield and J.-M. Lehn, *New J. Chem.*, 2012, **36**, 668–673.
53 Y. Xiang, A. J. Tong, P. Y. Jin and Y. Ju, *Org. Lett.*, 2006, **8**, 2863–2866.
54 Y. Xiang, M. Li, X. T. Chen and A. J. Tong, *Talanta*, 2008, **74**, 1148–1153.
55 X. T. Chen, Z. F. Li, Y. Xiang and A. J. Tong, *Tetrahedron Lett.*, 2008, **49**, 4697–4700.
56 N. Li, W. X. Tang, Y. Xiang, A. J. Tong, P. Y. Jin and Y. Ju, *Luminescence*, 2010, **25**, 445–451.
57 J. M. An, M. H. Yan, Z. Y. Yang, T. R. Li and Q. X. Zhou, *Dyes Pigm.*, 2013, **99**, 1–5.
58 J. M. An, Z. Y. Yang, M. H. Yan and T. R. Li, *J. Lumin.*, 2013, **139**, 79–83.
59 H. L. Li, J. L. Fan, F. L. Song, H. Zhu, J. J. Du, S. G. Sun and X. J. Peng, *Chem.–Eur. J.*, 2010, **16**, 12349–12356.
60 H. Li, J. Cao, J. Fan and X. Peng, *Tetrahedron Lett.*, 2013, **54**, 4357–4361.
61 H. G. Wang, Y. P. Li, S. F. Xu, Y. C. Li, C. Zhou, X. L. Fei, L. Sun, C. Q. Zhang, Y. X. Li, Q. B. Yang and X. Y. Xu, *Org. Biomol. Chem.*, 2011, **9**, 2850–2855.
62 H. N. Kim, S. W. Nam, K. M. K. Swamy, Y. Jin, X. Q. Chen, Y. Kim, S. J. Kim, S. Park and J. Yoon, *Analyst*, 2011, **136**, 1339–1343.
63 S. Mukherjee, S. Chowdhury, A. P. Chattopadhyay and H. Stoeckli-Evans, *Polyhedron*, 2010, **29**, 1182–1188.
64 S. Mukherjee, S. Chowdhury, A. K. Paul and R. Banerjee, *J. Lumin.*, 2011, **131**, 2342–2346.
65 S. Mukherjee, P. Mal and H. Stoeckli-Evans, *Polyhedron*, 2013, **50**, 495–501.
66 Y. Zhou, H. N. Kim and J. Yoon, *Bioorg. Med. Chem. Lett.*, 2010, **20**, 125–128.
67 (*a*) M. R. Ganjali, F. Faridbod, P. Norouzi and M. Adib, *Sens. Actuators, B*, 2006, **120**, 119–124; (*b*) F. Faridbod, M. R. Ganjali, B. Larijani, P. Norouzi, S. Riahi and F. F. S. Mirnaghi, *Sensors*, 2007, **7**, 3119–3135.

68 S. Anbu, S. Shanmugaraju, R. Ravishankaran, A. A. Karande and P. S. Mukherjee, *Dalton Trans.*, 2012, **41**, 13330–13337.
69 H.-G. Li, Z.-Y. Yang and D.-D. Qin, *Inorg. Chem. Commun.*, 2009, **12**, 494–497.
70 Z. C. Liao, Z. Y. Yang, Y. Li, B. D. Wang and Q. X. Zhou, *Dyes Pigm.*, 2013, **97**, 124–128.
71 S. Goswami, S. Chakraborty, S. Paul, S. Halder and A. C. Maity, *Tetrahedron Lett.*, 2013, **54**, 5075–5077.
72 S. Ulrich, A. Petitjean and J.-M. Lehn, *Eur. J. Inorg. Chem.*, 2010, 1913–1928.
73 L. N. Wang, W. W. Qin and W. S. Liu, *Inorg. Chem. Commun.*, 2010, **13**, 1122–1125.
74 S. Goswami, A. Manna, S. Paul, K. Aich, A. K. Das and S. Chakraborty, *Dalton Trans.*, 2013, **42**, 8078–8085.
75 L. L. Zhou, X. H. Zhang and S. K. Wu, *Chem. Lett.*, 2004, 850–851.
76 J. Shao, H. Lin, M. Yu, Z. S. Cai and H. K. Lin, *Talanta*, 2008, **74**, 1122–1125.
77 S. Z. Hu, Y. Guo, J. Xu and S. J. Shao, *Org. Biomol. Chem.*, 2008, **6**, 2071–2075.
78 Q. Li, Y. Guo, J. Xu and S. J. Shao, *J. Photochem. Photobiol., B*, 2011, **103**, 140–144.
79 R. K. Mishra, V. Kumar, U. Diwan, K. K. Upadhyay and P. K. R. Chowdhury, *J. Mol. Struct.*, 2012, **1027**, 167–174.
80 Y. Sun, Y. Liu and W. Guo, *Sens. Actuators, B*, 2009, **143**, 171–176.
81 Y. Sun, Y. L. Liu, M. L. Chen and W. Guo, *Talanta*, 2009, **80**, 996–1000.
82 X. Lv, J. Liu, Y. L. Liu, Y. Zhao, M. L. Chen, P. Wang and W. Guo, *Org. Biomol. Chem.*, 2011, **9**, 4954–4958.
83 S. Anbu, S. Kamalraj, C. Jayabaskaran and P. S. Mukherjee, *Inorg. Chem.*, 2013, **52**, 8294–8296.
84 O. G. Tsay, S. T. Manjare, H. Kim, K. M. Lee, Y. S. Lee and D. G. Churchill, *Inorg. Chem.*, 2013, **52**, 10052–10061.
85 H. Y. Lee, X. L. Song, H. Park, M. H. Baik and D. Lee, *J. Am. Chem. Soc.*, 2010, **132**, 12133–12144.
86 H. Yang, H. S. Song, Y. C. Zhu and S. P. Yang, *Tetrahedron Lett.*, 2012, **53**, 2026–2029.
87 Y. H. Kim, M. G. Choi, H. G. Im, S. Ahn, I. W. Shim and S.-K. Chang, *Dyes Pigm.*, 2012, **92**, 1199–1203.
88 X. F. Yang, P. Liu, L. P. Wang and M. L. Zhao, *J. Fluoresc.*, 2008, **18**, 453–459.
89 P. Wang, J. Liu, X. Lv, Y. L. Liu, Y. Zhao and W. Guo, *Org. Lett.*, 2012, **14**, 520–523.
90 L. F. Sgobbi, V. D. Pinho, M. F. Cabral, A. C. B. Burtoloso and S. A. S. Machado, *Sens. Actuators, B*, 2013, **182**, 211–216.
91 M. E. Belowich and J. F. Stoddart, *Chem. Soc. Rev.*, 2012, **41**, 2003–2024.
92 (*a*) Y. Yang, R. P. Hughes and I. Aprahamian, *J. Am. Chem. Soc.*, 2012, **134**, 15221–15224; (*b*) X. Su, M. Liptak and I. Aprahamian, *Chem. Commun.*, 2013, **49**, 4160–4162; (*c*) X. Su and I. Aprahamian, *Org. Lett.*, 2013, **15**, 5952–5955.